ICARUS **134,** 187–206 (1998)
ARTICLE NO. IS985956

A Thermal Model for the Differentiation of Asteroid 4 Vesta, Based on Radiogenic Heating

Amitabha Ghosh and Harry Y. McSween, Jr.

Department of Geological Sciences, University of Tennessee, Knoxville, Tennessee 37996–1410

Received October 21, 1997; revised April 22, 1998

A finite element code has been developed to model the thermal history of Asteroid 4 Vesta. This is the first attempt to model the thermal history of a differentiated asteroid through core and crust formation and subsequent cooling until geochemical closure is attained. The results of the simulation are consistent with chronological measurements and other constraints provided by cumulate and noncumulate eucrites believed to have been derived from Vesta. The work solves two major problems with the hypothesis of heating by decay of ^{26}Al, an extinct radionuclide, postulated to be a plausible heat source in the early Solar System. First, the model demonstrates that it is possible to keep the mantle of Vesta hot for ~100 Ma, thereby explaining the observed difference in ages between cumulate and noncumulate eucrites. Second, the simulation offers a possible explanation of why detectable excesses of ^{26}Mg (the decay product of ^{26}Al) are not observed in noncumulate eucrites. The simulation draws a model chronology of Vesta and predicts times (relative to CAI formation) for accretion at 2.85 Myr, core formation at 4.58 Myr, crust formation at 6.58 Myr, and geochemical closure at ~100 Myr for a H-chondrite asteroidal bulk composition. Decay of ^{60}Fe is found to cause no perceptible difference in the thermal history of Vesta, even when sequestered into a central core. Although chondritic xenoliths have not been described in HED igneous lithologies, the thermal model suggests the possibility that a veneer of unmelted near-surface material should remain.

Key Words: **Vesta; thermal modeling; eucrites; diogenites; howardites.**

INTRODUCTION

Asteroid 4 Vesta, with a radius of 265 km, is situated at a mean heliocentric distance of 2.36 AU. Because of its large size and its brightness near opposition (once every 18 months), Vesta is one of the most widely studied minor bodies in the Solar System. Its reflectance spectrum closely resembles the laboratory spectra of HED (howardite–eucrite–diogenite) meteorites and suggests that Vesta was either the source for these meteorites or that it has undergone a history similar to that of the HED parent body (McCord *et al.* 1970, Drake 1979). Originally, it was thought that Vesta's orbital location was not propitious for providing a significant flux of meteorites in Earth-crossing orbits (e.g., Wetherill 1987). However, the discovery of a cluster of small V-type asteroids (objects with albedos and absorption features similar to Vesta) having orbits extending from the region around Vesta to the edge of the 3:1 mean motion commensurability with Jupiter at 2.5 AU (Binzel and Xu 1993) has resolved this problem. The small asteroids have been interpreted as ejecta from a large impact onto Vesta (Binzel and Xu 1993), and ejecta reaching the 3:1 resonance can be readily transferred into Earth-crossing orbits (e.g., Wisdom 1985, Farinella *et al.* 1993). The absence of another large V-class asteroid and the demonstration of a delivery mechanism to transport meteorites from Vesta to Earth add a new perspective to studies of HED meteorites. Vesta is now generally recognized as a third specific extraterrestrial body (in addition to the Moon and Mars) for which actual rock samples are available for laboratory analysis. Petrogenetic, geochemical, and chronologic constraints on the formation of HED meteorites allow the thermal history of Vesta to be modeled with more assurance than for other differentiated asteroids.

The importance of studying the thermal evolution of Vesta is twofold: to gain insights into nebular processes and to understand the processes of core and crust formation in protoplanetary bodies. In the context of early Solar System history, Vesta is perhaps more valuable than the other larger bodies for which we have samples. Isotopic closure on Vesta took place between ~5 and a few hundred Myr after the formation of the Solar System, so it bears the thermal signature of the pervasive heating event that caused melting, metamorphism, and aqueous alteration in planetesimals before their accretion into planets. Planetary processes like core formation and basaltic volcanism operated on Vesta, and already differentiated planetesimals are thought to have been a major component of the materials that accreted to form the terrestrial planets (Taylor and Norman 1990).

Most thermal models for chondritic asteroids (e.g., Miyamoto *et al.* 1981, Grimm and McSween 1989, Bennett and

0019-1035/98 $25.00

McSween 1996) have focused on subsolidus temperature excursions to explain thermal metamorphism and aqueous alteration. In modeling the thermal history of a differentiated asteroid, it becomes important to account for the latent heat of fusion and the increased specific heat of melts, as well as to consider the possible effects of the redistribution of short-lived radionuclides (^{26}Al and ^{60}Fe) during differentiation. Haack *et al.* (1990) and Warren *et al.* (1991) modeled the cooling histories of differentiated asteroids using long-lived radionuclides (U, Th, K) as heat sources but assumed that the body was already stratified into a crust, a mantle, and a core at the beginning of the simulation. They assumed regolith and megaregolith thicknesses of up to 1 and 11%, respectively, of the asteroid radius which requires values of cratering rates at odds with numerical studies of regolith formation on Vesta (Housen *et al.* 1979, Langevin and Maurette 1980). Even if accretion rates were higher in the first few Myr, the regolith would be vulnerable to destruction by extrusive volcanism on Vesta. Because of these uncertainties, we have not included the thermal effects of an insulating regolith, although we acknowledge that howardites indicate the presence of some regolithic materials of unknown thickness on Vesta. Moreover, Haack *et al.* (1990) did not take into account short-lived radionuclide decay or electromagnetic induction as heat sources. Further, their results cannot be anchored to absolute time with respect to CAI formation. The detailed thermal model presented here traces the thermal history of the asteroid, through the stages of core formation and surface igneous activity, until it cooled to temperatures of isotopic closure. The simulation evaluates a model in which the degree of partial melting is $\leq$25%, compatible with classical views of the petrogenesis of HED meteorites (Mason 1962, Stolper 1977). Since the amount of partial melting is restricted to 25%, the thermal model cannot be used to study scenarios with very high degrees of melting (Righter and Drake 1997, Ruzicka *et al.* 1996).

MODEL CONSTRAINTS PROVIDED BY HED METEORITES AND 4 VESTA

HED Petrology and Chronology

Eucrites are basaltic achondrites consisting predominantly of pigeonite and plagioclase, with minor amounts of silica polymorphs, ilmenite, chromite, troilite, kamacite, phosphates, zircon, and occasionally olivine (Duke and Silver 1967, Lovering 1975, Takeda *et al.* 1983, Treiman and Drake 1985). Most eucrites are monomict breccias. Polymict eucrites are composed of clasts of various eucrite and cumulate eucrite lithologies. Noncumulate eucrites are believed to be near-surface basalts, whereas cumulate eucrites are thought to be plutonic rocks. Many eucrites show homogenization of originally zoned pyroxene grains (Miyamoto *et al.* 1985) and clouding of pyroxene and plagioclase grains by finely disseminated inclusions (Harlow and Klimentidis 1980), indicating recrystallization during thermal annealing. Diogenites are brecciated orthopyroxenites containing minor olivine (Mason 1962, Gooley and Moore 1976, Hewins 1981). Their coarse grain sizes and homogeneous pyroxenes indicate crystallization in plutonic environments. Howardites are polymict regolith breccias made up of clasts of eucrites, diogenites, and other related rocks (Bunch 1975, Dymek *et al.* 1976, Desnoyers and Jerome 1977, Ikeda and Takeda 1985). In contrast to polymict eucrites, howardites have a greater diogenite component (Labotka and Papike 1980).

Eucrites, diogenites, and howardites lie on a common oxygen isotope fractionation line (Clayton and Mayeda 1993), supporting the idea that they formed on the same parent body. However, the exact petrologic relationship between eucrites and diogenites is a matter of debate. According to one scenario (e.g., Grove and Bartels 1992), eucrites and diogenites are highly fractionated products of a single magma. A competing idea is that eucrites are partial melts and diogenites crystallized from magmas produced from the same source region at greater degrees of melting (Stolper 1977). Jurewicz *et al.* (1995) argued that if eucrites and diogenites derive from the same parent body, this asteroid must be chemically heterogenous.

The radiometric ages of HED meteorites cluster around 4.4–4.6 Ga, according to Rb–Sr, Sm–Nd, and U–Pb geochronology (Papanastassiou and Wasserburg 1969, Tatsumoto *et al.* 1973, Allegre *et al.* 1975, Lugmair and Scheinn 1975, Birck and Allegre 1978, Basaltic Volcanism Study Project 1981, Jacobsen and Wasserburg 1984, Nyquist *et al.* 1986, Tera *et al.* 1997). A few younger ages have been reported, some as low as 2.6 Ga. The older ages are believed to be crystallization ages, whereas the younger ages denote resetting by shock, as is supported by a wide spectrum of ^{40}Ar/^{39}Ar ages (Bogard 1995). Sm-Nd chronology of cumulate eucrites indicates relatively young ages of 4.46 to 4.41 Ga (Tera *et al.* 1989, Jacobsen and Wasserburg 1984) compared with the 4.52- to 4.56-Ga ages obtained for noncumulate eucrites (Birck and Allegre 1978, Carlson *et al.* 1988). Various workers interpret the younger ages of cumulate eucrites as representing either the time of crystallization or post-metamorphic cooling to isotopic closure. In either case, it is necessary to maintain high temperatures inside Vesta for ~100 Myr after formation of Ca–Al-rich inclusions (CAIs), thought to be the first-formed solids in the Solar System.

Surface Geology of Vesta

Geologic mapping of Vesta using the Hubble Space Telescope (HST) during the 1994 apparition showed to be geologically dichotomous (Binzel *et al.* 1997, Gaffey 1997). The eastern hemisphere is dominated by units composed

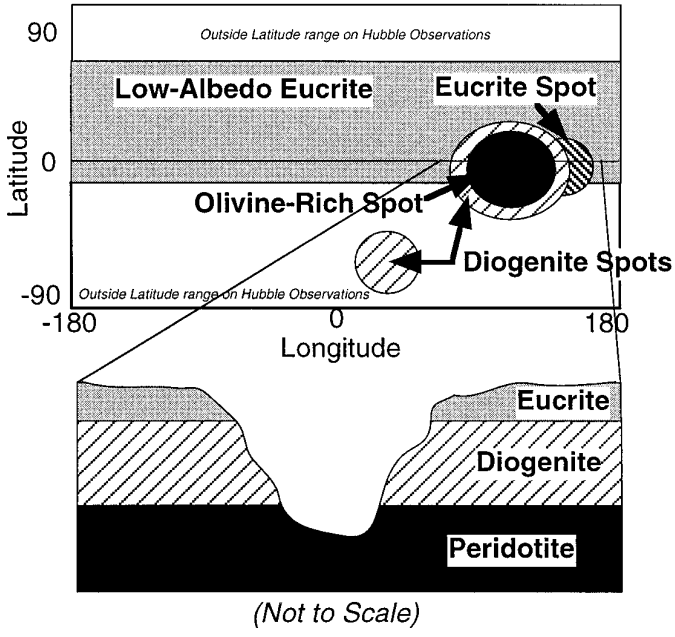

FIG. 1. A hypothetical cross section of the equatorial part of Vesta drawn from the interpretive lithologic maps of Gaffey (1997) and Binzel *et al.* (1997).

of magnesium-rich and calcium-poor pyroxene interpreted to be similar in composition to diogenites. The western hemisphere is dominated by an iron-rich and calcium-rich pyroxene analogous to eucrites and an olivine component. The eastern hemisphere is interpreted to consist of impact-excavated plutonic rocks, whereas the western hemisphere is believed to be composed of surfacial lava flows. Hubble Space Telescope WBFPC2 images (Thomas *et al.* 1997a) during the 1996 apparition show that a huge crater, of 450 km in diameter and ~8 km in depth, with elevated rims (8–14 km high) and a central peak (~13 km high), occur in the southern hemisphere near the south pole. A color ratio variation is observed indicating a possible transition from pyroxene to olivine to high Ca pyroxene with increasing topographic depth in the crater (Thomas *et al.* 1997a). That study found several other craters in Vesta that are 150 km in diameter and a few km deep. A hypothetical cross section at the equator is shown in Fig. 1.

Diameter and Density of Vesta

The International Astronomical Satellite (IRAS) Asteroid and Comet Survey measured the radius of Vesta to be 250 ± 12 km (Tedesco 1989). Thomas *et al.* (1997b), using the Wide Field Planetary Camera (WBFPC2) and the HST, determined the radius of Vesta at 265 ± 7 km. In our thermal model, we use a radius of 270 km which is within the error bars of the measurement by Thomas *et al.* (1997b). The shape of Vesta is slightly oblate spheroid with an equatorial axial ratio of 1.065 ± 0.01 (Drummond *et al.* 1988) and is assumed to be spheroidal in this work. The fact that Vesta and Asteroid 197 Arete approach within 0.04 AU every 18 years has been used to determine the mass of Vesta from its gravitational effect on Arete. The mass of Vesta as determined by this method (Hertz 1968) is $2.746 \pm 0.24 \times 10^{20}$ kg. Schubart and Matson (1979) estimated a mass of $2.75 \pm 0.25 \times 10^{20}$ kg, while Standish and Hellings (1989) calculated $2.9 \pm 0.58 \times 10^{20}$ kg. Using the measurements of Thomas *et al.* (1997b) and Standings and Hellings (1989), the calculated density of Vesta is 3.7 g/cm^3 (between 3.2 and 4.1 g/cm^3, considering the error bars). This huge uncertainty makes it impossible to estimate reliably the bulk density, the size of the core, or the metal content of Vesta. The mean opposition distance of Vesta from the Sun is taken to be 2.36 AU (Millis and Elliot 1979).

Bulk Composition

Mean density estimates for Vesta (3.3 ± 1.5 g/cm^3, Schubart and Matson 1979) have too great an uncertainty to enable a reliable calculation of the proportion of metal. Moment of inertia measurements of Vesta, which could constrain the size of the core, have not been made. Consolmagno and Drake (1977) determined the bulk composition of Vesta from rare earth element modeling to be chondritic, but were unable to estimate the amount of metal. Boesenberg and Delaney (1997) suggested a mixture of 65% H-chondrite and 35% CM-chondrite as the bulk chemical composition of Vesta on the basis of matching oxygen isotopes. Mixing of CM- and H-chondrites is not a unique solution. As pointed by Clayton (1993), any known oxygen isotopic composition of achondrites, including HED meteorites, can be fixed by mixing C3-chondrites (high ^{16}O endmember), C1-chondrites (high ^{18}O endmember), and ordinary chondrites (low ^{16}O endmember). Needless to say, other combinations are possible (e.g., C2- and H-chondrites). Moreover, in order to balance the bulk composition, such calculations require volatile depletion by vaporization to be invoked, a process not supported by K isotope measurements (Humayun and Clayton 1995). Experiments by Boesenberg and Delaney (1997) indicate a better match in Fe/Mn ratios with their favored precursor composition than with a Murchison (CM chondrite) analog (experiments by Jurewicz *et al.* 1995), although the latter gives a better match for observed Na content in eucrites. In any case, an oxygen isotopic signature may essentially depict the isotopic fractionation within a certain *portion* of the nebula and need *not* correspond to a particular chondrite type or a mixture of various chondrite types.

Holzheid and Palme (1996) performed experiments to constrain metal–silicate partition coefficients and concluded that eucrites were generated by partial melting of

a source region with an approximate metal–silicate ratio of H chondrite. In our simulation, it is assumed that the feeding zone of Vesta had a composition of H chondrite. The amount of metal in our model is similar to that used by Driebus *et al.* (1997) who assumed that Fe and Ni were present in CI chondrite abundances relative to Si. The radius of the core used in the thermal model (123 km) is exactly equal to the core radius deduced by Driebus *et al.* (1997). In order to evaluate the dependence of thermal history on bulk composition, the code has also been run using L and LL chondrite compositions.

Relative Timing of Core and Crust Formation

The timing of core formation (relative to igneous activity) on Vesta might be inferred from siderophile element measurements of HED meteorites (Newsom 1985, Hewins and Newsom 1988), though this has not provided a definitive answer. Constant ratios of W, a moderately siderophile element, to Mo, a highly siderophile and chalcophile element, have been cited as evidence that the HED parent body experienced a core-forming event before igneous fractionation (Newsom 1985). Data for the incompatible siderophile element P further support this hypothesis (Newsom and Drake 1983). However, Newsom (1996) has recently reported that abundances of W, normalized to La, are higher for Pomozdino, Y 74450, Stannern, and Bouvante than for most other eucrites. It is possible that this variability is due to differences in bulk mineral-melt partition coefficients of W in HEDs, resulting from either igneous fractionation in the *presence* of metal or heterogeniety in the source region of eucrites.

In addition to trace element modeling, theoretical and experimental studies offer other ways of studying core formation on Vesta. Theoretical models deal with (1) the physics of metal segregation by porous flow using Darcy's Law (e.g., Turcotte and Schubert 1982), (2) empirical relations deduced from experiments, relating yield strength of silicate liquid to fraction of metallic globules present (Taylor 1992), (3) mechanisms for growth of metal grains such as Ostwald ripening (Greenwood 1969), or (4) the feasibility of convection (Herndon and Herndon 1977). The experimental approach involves melting experiments using chondritic compositions (e.g., Larimer 1995). These considerations lead to two schools of thought regarding core separation. One possibility is that core formation requires high degrees (~50%) of silicate partial melting (Stevenson 1990, Taylor 1992). A competing model, based on the experimental data of Larimer (1995), suggests that melt migration can be realized at lower degrees of partial melting, and is essentially instantaneous. Observation that metal-sulfide eutectic liquids separated at low degrees of melting in the acapulcoite–lodranite parent asteroid (e.g., Middlefelt *et al.* 1996, McCoy *et al.* 1996) favors the latter, but separation of more metal-rich liquids may be more difficult. Neither approach accounts for the rate of melt generation which, in turn, relates to the thermal environment in the asteroidal interior. For example, latent heat is required to melt the metal-sulfide liquid. How fast the metal sulfide liquid *moves* at a particular depth will be determined also by how fast it *melts*, which in turn is determined by the amount of heat that is supplied by ^{26}Al decay and the amount of heat brought into or lost to adjacent layers.

When the eutectic temperature of the Fe–FeS system (1213 K) is reached at a particular depth in Vesta, a melt of eutectic composition is generated. So long as the melt stays where it formed, there is further melting *if* the ^{26}Al content of the melt + residue is high enough to provide the required latent heat. If, however, the metal-sulfide liquid separates from the residue, the residue will melt further because the residue has a greater Al (hence ^{26}Al) abundance than the Al abundance of the melt + residue. The metal-sulfide melt can separate from the residue by moving downward toward the center of the asteroid or by moving out of the pore spaces in the rock. The former will cause melting in all rocks at that depth, and the latter will cause melting in pockets due to mosaic equilibrium, which results in a positive feedback mechanism: the greater the amount of metal-sulfide melt drained away, the greater the ^{26}Al concentration in the residue, which causes the residue to melt even further. A cascading effect results, where melt generation and segregation cause the residue to melt further. So, *if physical factors were propitious*, thermal considerations point to rapid core separation on Vesta, even before the onset of silicate partial melting.

The timing of core formation relative to igneous activity leads to a bigger problem: that of the sequence of core and crust formation which, in turn, determines the distribution of radionuclides in time and within the asteroidal interior (see Fig. 2). A homogeneous asteroid (1) may or may not undergo core separation when temperatures reach the Fe–FeS eutectic (2 and 3, respectively). Core and crust formation might not take place in spite of silicate and sulfide melting (4). Crust formation may take place without metal segregration (5). Core formation may occur without crust formation (6). Both core and crust formation may take place (7). Hence, sequence 1–3–7 is conceivable in a scenario where melt migration is possible at low degrees of partial melting (Larimer 1995) and represents the situation proposed by Hewins and Newsom (1988) wherein core separation precedes silicate melting. Sequence 1–2–7 is compatible with a scenario requiring high degrees of silicate partial melting for metal segregation (e.g., Stevenson 1982). Two of these possibilities are considered in this work: endmember A in which crust formation takes place after core formation (1–3–7), and endmember B where

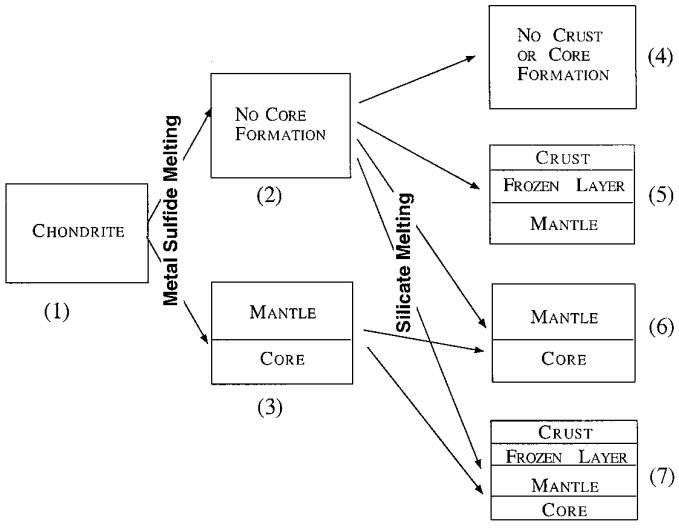

FIG. 2. Possible sequences of core and crust formation on a generic asteroid undergoing silicate melting. Uncertainty in the timing and duration of core formation with respect to onset of silicate melting and crust formation gives rise to a host of possibilities. The scenarios shown are endmembers: (2) all the metal and sulfide migrate to form a central core; (3) no metal and sulfide migrate to the center. In reality, it is possible that something between (2) and (3) takes place; i.e., some metal-sulfide migrates to the center, whereas the rest remains in the mantle. The configuration of Vesta at various times is important in a thermal model because differentiation causes redistribution of ^{26}Al, the heat source. In the thermal model presented, we study scenarios (1)–(3)–(6) and (1)–(3)–(7). The frozen layer in (7) may or may not survive depending on the degree of partial melting in Vesta.

core formation takes place but crust segregation does not occur (1–3–6).

Composition and Size of the Core, Mantle, and Crust

Our ignorance of the initial composition of Vesta makes it difficult to calculate the composition of the core. We assume that all metal and troilite present in the precursor chondritic mantle migrate to form a core. Thus, the size of the core produced for different initial compositions is different. Precursor compositions of H, L, and LL chondrite yield cores of 123, 108, and 90 km radius, respectively. Also, the proportion of Fe metal (relative to FeS) in the core decreases from H to LL chondrite. Furthermore, there can be intermediary stages between model endmembers A and B. For example, the temperature at which metal segregation takes place will dictate the composition of the Fe–FeS liquid. If metal segregation takes place near the Fe–FeS eutectic, the composition of the core will correspond to the eutectic of the Fe–FeS system (31 wt% S), whereas if metal segregation takes place at higher temperatures, the core will be richer in Fe.

Jones (1984) estimated a composition of the mantle of the HED parent body based on olivine–liquid partition coefficients for Sc, Mg, and Si. He concluded that the mantle could be approximated by a mixture of 25% eucrite and 75% olivine. In our model, the composition of the crust is assumed to be a model eucrite (calculated by Jones 1984) and the composition of the barren mantle is assumed to be olivine of the composition calculated by Jones (1984) (see Appendix). This rather simplistic model for the internal structure of the HED meteorite parent body does not take into account the constraints from recent work on the experimental petrology of Vesta by Jurewicz *et al.* (1995), who conclude that the HEDs cannot be linked to the same parent body unless the body is chemically heterogeneous. Furthermore, Jones (1984) does not consider the existence of a possible diogenite layer in his model. Nevertheless, in the absence of better models and in recognition of the fact that the structure of Vesta is as yet unknown, compositions calculated by Jones (1984) are used. A mass ratio of 75% olivine and 25% eucrite is used to calculate the relative proportion of the mantle and the crust.

Ideally, the composition of the core, mantle, and crust, when multiplied by their mass fractions, should match the abundance of each element in the original composition. This does not happen in the simulation. The initial composition of Vesta is assumed to have the composition of an H, L, or LL chondrite. A core is separated from this homogenous asteroid, and the size and composition of the core in the model are determined by the abundance of metal and troilite in the precursor material. The composition and volume proportion of the mantle and the crust, on the other hand, are estimated from Jones (1984) and the mass proportion is set to 3 : 1. Significantly, the size of the core will also determine the proportional enrichment of ^{26}Al in the precursor mantle after core separation, and it was not possible to incorporate this into the thermal model. The Al abundance in the precursor mantle calculated by Jones (1984) is used in the thermal model.

Instantaneous Accretion, Core and Crust Formation

In a previous abstract (Ghosh and McSween 1996), we attempted to model the progressive growth of Vesta during radionuclide decay. An erroneous conclusion from that work—that accretion of cold material would offset the heat generated by radioactive decay—is an artifact of the algorithm used to remap the nodes during asteroidal growth. In this paper, we assume instantaneous accretion, as have prior thermal models (e.g., Minster and Allégre 1979, Wood 1979, Miyamoto *et al.* 1981, Grimm and McSween 1989, Haack *et al.* 1990, Bennett and McSween 1996).

As discussed earlier, thermal considerations indicate that core formation on Vesta was rapid if physical factors were favorable. For the purposes of our thermal model, we take core formation to be instantaneous. We assume

that the entire metal and sulfide content of the chondritic precursor material drained to form the core before the initiation of silicate partial melting. As previously discussed, this simplification is supported by trace element modeling (Newsom 1985, Newsom and Drake 1983), some experimental studies (Larimer 1995), and the observation in lodranites that migration of a metal-sulfide melt was initiated at low degrees of partial melting (McCoy *et al.* 1996). In the thermal model, melting is initiated at the eutectic of the Fe–FeS system (1213 K: Larimer 1995) and terminated after a 20 K temperature rise at 1233 K. The former temperature is termed the ''metal-sulfide solidus'' in this paper and the latter as the ''metal-sulfide liquidus.'' The entire latent heat for melting metal and sulfide in the precursor chondrite is assumed to be expended in the temperature range between the solidus and the liquidus.

Silicate melt generation in the simulation is also rapid. If it is assumed that 25% partial melting of the primordial mantle generated the crust (Jones 1984), the thermal model shows that this fraction of melt is generated within about 0.5 Myr, resulting from the tremendous heat flux due to ^{26}Al decay when silicate melting is first initiated. Eucritic melting is assumed to initiate at 1443 K based on the experimental results of Stolper (1977) and 25% partial melting is accomplished by 1463 K. The former temperature is referred to the ''silicate solidus'' and the latter is referred to as the ''silicate liquidus'' (although we recognize that it does not correspond to the mantle liquidus temperature). The temperature ''windows'' for silicate and sulfide melting are simplifications for the code. This simplification will not make a perceptible difference in the whole-body thermal history because the latent heat would have to be supplied in any case to cause silicate and sulfide melting—it is merely constrained to a certain temperature window for convenience in coding. Once a critical mass of magma accumulates at a particular depth, it will migrate nearly instantaneously to the surface (Wilson and Keil 1996). Crust formation is assumed to be instantaneous in the thermal model.

Initial and Ambient Temperature of Vesta

There are two possible approaches in determining the nebular temperature, and its variation with time and heliocentric distance: hydrodynamic and equilibrium condensation models. Neither model has been anchored to meteorite evidence (A. Boss, pers. commun., 1996). In other words, it is not yet possible to correlate precise time scales drawn from theoretical models and high-resolution chronometers from meteorites. Neither is it possible to anchor theoretical results to meteoritic evidence at any particular time for varying heliocentric distance. The temperatures arrived at from various nebular models (reviewed by Wood and Morfill 1988) range from 1000 K (Cameron and Pine 1973) to 160 K at 3 AU (Hayashi *et al.* 1985). Boss (1990) suggested that midplane temperatures in the disk rose to about 1500 K inboard of 3 AU, decreased linearly to 10 K between 3 and 20 AU, and stayed constant at 10 K beyond 20 AU. Weidenshilling (1988) calculated a temperature of 300 K at a distance of 2.77 AU. However, there is a problem in determining the absolute time (with reference to the age of CAIs) at which such temperatures might have been prevalent. Equilibrium condensation models suggest a range of formation temperatures in the asteroid belt. Lewis (1974) gave a formation temperature of 190–200 K for Vesta using different adiabats and pressures in the solar nebula. Barshay and Lewis (1976) calculated a temperature of ~400 K using a simplified condensation sequence after Grossman (1972).

There is no unique initial temperature of Vesta that could be arrived at from any of these approaches. Therefore, a temperature gradient in the nebula is calculated from a perspective which is simpler than the rigorous models, but yields a temperature in the range expected from either approach. On the basis of inferred thermal stratification in the asteroid belt, Bell *et al.* (1989) proposed that hydrated asteroids occur outboard of 2.7 AU. In this work, it is assumed that ice condenses (so that it can be incorporated into the accreting planetesimals) at 2.7 AU. The value of the solar constant at the time of asteroidal accretion is recalculated by substituting the value for a temperature of 273 K at 2.7 AU. From the value of the solar constant, a temperature profile in the asteroid belt is evaluated. This gives an initial temperature of Vesta (at 2.36 AU) to be 292 K. (In order to determine the effect of initial temperature on the chronology obtained from the model, we decreased in the initial temperature from 292 to 270 K. This increased the time required for core and crust separation by 0.09 Myr.) Because the variation of temperature with time in the solar nebula is unconstrained, it is assumed that the ambient temperature equals the initial temperature throughout the simulation, i.e., until 130 Myr after CAI formation. The ambient temperature possibly decreased with time, which would have expedited heat loss from the body. This would produce a slight decrease in the surface temperature and small differences in the temperature profile with depth inside Vesta.

Heat Source for Vesta

The heat source that caused melting and differentiation of the HED parent body is still unclear. Two mechanisms are accepted as plausible by many workers—electromagnetic induction heating and heating by rapid decay of ^{26}Al. Both mechanisms have problems (Wood and Pellas 1991). Most models of electromagnetic induction heating assume that solar wind in the T-Tauri phase swept by the planetesimals, a scenario no longer believed to be true

(e.g., Edwards *et al.* 1989). The T-Tauri outflow is now thought to have been poleward collimated, i.e. perpendicular to the plane of the accretionary disk. It is also argued that the solar wind flux may have been anisotropic, whereas induction models assume the flux to be isotropic. Some advocates (Herbert 1989) have been criticized (e.g., Wood and Pellas 1991) for using an unrealistic value of the Sun's rotational velocity during the T-Tauri phase. The dependence of electrical conductivity on temperature and material, a very crucial parameter in electromagnetic induction heating, is poorly known.

The absence of excess radiogenic ^{26}Mg in noncumulate eucrites like Juvinas and Pasamonte (Schramm *et al.* 1970) and the difficulty in explaining an apparent time interval of ~100 Myr between cumulate and noncumulate eucrites (if their ages are taken to be igneous crystallization ages) are some of the problems raised against the hypothesis of ^{26}Al decay as a heat source (Wood and Pellas 1991). Grimm and McSween (1989) showed that ^{26}Al heating could explain aqueous alteration in ice-bearing planetesimals, and Bennett and McSween (1996) updated the ordinary chondrite asteroid thermal model of Miyamoto *et al.* (1981) based on ^{26}Al decay, using recently derived thermal parameters and new constraints from U–Pb studies from Göpel *et al.* (1994). Grimm and McSween (1993) were also able to model quantitatively the apparent thermal stratification in the asteroid belt (sometimes cited as supporting electromagnetic induction heating) using ^{26}Al heating in an accretionary model. A comprehensive review of ^{26}Al distribution in meteoritic materials (MacPherson *et al.* 1995) concluded that this radionuclide was widespread in the early Solar System and that the timing of parent body accretion was the dominant factor in determining its efficacy as a heat source. The question of the heat source for the HED parent body is still unsettled, though recent explanations for several problems with the ^{26}Al hypothesis and certain points raised against electromagnetic induction heating by Wood and Pellas (1991) may favor ^{26}Al.

^{60}Fe decay was proposed as a possible heat source by Shukolyukov and Lugmair (1993) on the basis of measurements of its ^{60}Ni decay product in Juvinas. Using relative chronology, they calculated the initial ratio of ^{60}Fe/^{56}Fe to be $\sim 10^{-6}$ at the time of CAI formation. Because of the high abundance of Fe in the Solar System and the high decay energy of ^{60}Fe (3.04 MeV), it was proposed that ^{60}Fe could be a planetary heat source. However, new data seem to indicate that the ratio of ^{60}Fe/^{56}Fe at the time of CAI formation was only $\sim 2 \times 10^{-8}$ (Shukolyukov and Lugmair 1996). Even so, it may be interesting to evaluate whether ^{60}Fe decay can cause heating when Fe is segregated in the core. Both ^{26}Al, with an initial ratio of 5×10^{-5} (MacPherson *et al.* 1995) at the time of CAI formation, and ^{60}Fe, with an initial ratio of 2×10^{-8} at the time of CAI formation, are used as heat sources in this work.

THERMAL MODEL OF VESTA

Chronologically, the thermal evolution of Vesta can be divided into three stages. The heat transfer equation (Appendix) is solved for an asteroid using decay of radioactive ^{26}Al and ^{60}Fe as heat sources. Accretion is assumed to be instantaneous, and a radiation boundary condition is used to approximate heat loss from the body. Thermal diffusivity and specific heat are recalculated for each temperature and rock type. A summary of the assumptions for each stage is given in Table I and explanations are provided in the previous section or in the Appendix.

Stage 1: Radiogenic Heating of the Homogeneous Asteroid until Core Separation

Stage 1 starts at 2.85 Myr after CAI formation with a homogeneous chondritic asteroid of radius 270 km having an initial temperature equal to that of the ambient nebula. The asteroid is observed to heat with time, maintaining an almost uniform temperature from the center to a depth of ~30 km, above which a steep gradient develops toward the surface (Figs. 3a and 4a). Eventually, Fe–FeS melting (assumed to take place between solidus and liquidus—see previous section) is completed in the whole asteroid except in the near-surface layers above a depth of ~30 km, which stay unmelted. Because we observe in our model that Fe–FeS melting in almost the whole asteroid except a 30-km shell is accomplished at about the same time, we feel that there is no compelling reason to believe why core separation, a process driven by gravity and unaffected by whether the near-surface layers of the asteroid have undergone metal silicate melting, should not proceed. Thus, we set a depth ''trigger'' at 30 km in our model and we assume that core formation is triggered as soon as temperatures at this depth reach the liquidus of the Fe–FeS system (i.e., the temperature when all the Fe–FeS melting is completed), taken to be 1223 K. On reaching the ''trigger,'' metal separation to form a core is assumed to be instantaneous, marking the end of stage 1.

Stage 2. Further Heating of the Mantle until Crust Formation

Stage 2 begins at 4.58 Myr after CAI formation, with a partly differentiated object consisting of a mantle and a core. The absolute concentration of Al in the mantle has risen noticeably, compared with the initial composition, from 1.13 to 1.69 wt%. Heat generation from ^{26}Al decay is revitalized in the mantle, and ^{60}Fe is segregated within the core. However, an increase in the absolute concentration of Fe is not found to be adequate to cause perceptible

TABLE I
Summary of the Evolution of Vesta through Stages 1 to 3

	STAGE-1	STAGE-2	STAGE-3
Stratification	Homogenous	Precursor Mantle, Core	Crust,Mantle & Core
Composition	H- Chondrite	Precursor Mantle=25% eucrites+75% Olivine, Core=Fe, FeS & Ni	Crust=eucrite, Mantle=Olivine, Core=Fe,FeS+Ni
Al Abundance (wt. %)	1.13%	Precursor Mantle=1.69%, Core=0.	Crust=6.88%, Mantle=0., Core=0.
Fe Abundance (wt. %)	24%	Precursor Mantle=19.6%, Core=89.3%	Crust=14.6%, Mantle=21.2%, Core=89%
Density (kg/m3)	3500	Precursor Mantle=3500, Core=7540	Crust=2700, Mantle=3500, Core=7540
Approx. Temprature range	400 K to liquidus of Fe-FeS system	Liquidus of Fe-FeS system to basalt liquidus	Around basalt liquidus and below
Absolute time after CAI formation at the end of the stage	4.58 Ma	6.58 Ma	130 Ma
Heating mechanism	26Al	Precursor Mantle=26Al; Core=60Fe	Crust=26Al for ~4Ma, Mantle=none, Core=none

heating from ^{60}Fe decay, because the initial abundance of ^{60}Fe is so low at the outset (Shukolyukov and Lugmair 1996). The core has no ^{26}Al and effectively no thermal contribution from ^{60}Fe decay. Hence, the increase in the temperature of the core is arrested while the mantle continues to heat (Fig. 3b and 4b). Notice that in Fig. 3a the time–temperature–radius surface becomes parallel to the time-radius plane after ~5 Myr, for radii less than ~100 km. At any particular time during this stage, the temperature of the core (radius <123 km) is less than the temperature of the mantle directly above it (Fig. 4b). This creates a reverse thermal gradient inside Vesta, where temperature decreases with depth. In terms of cooling history, this means that not only is heat loss from the core prevented, but some heat, in fact, flows downward into the core by thermal diffusion from the overlying mantle. The reverse gradient does not dissolve until ~100 Myr after CAI formation, after which time heat loss from the core is revived.

Temperatures in the mantle reach 1463 K (i.e. the temperature at which 25% partial melting of the mantle is accomplished—see previous section), but no melting takes place in the outer shell of thickness 30 km. It is possible to set a depth which triggers instantaneous crust formation as soon as the temperature reaches 1463 K (as was done in stage 1 for core formation). However, if the depth is too great the Al-rich eucritic crust would undergo tremendous heating (to ~2000 K), which seems implausible on the basis of meteoritic evidence (Jones *et al.* 1996). If the cut-off depth is too shallow, a temperature of 1463 K may never be attained (thereby not forming a crust in the model), though temperatures in the deeper mantle are high enough to cause complete melting. It is uncertain how much of the silicate melt penetrates the unmelted outer shell and erupts onto the surface to form a crust versus how much solidifies *in situ* or during ascent through the unmelted carapace. Crust formation on Vesta was probably not instantaneous. Instead, there may have been a short period of time (~0.5 Myr) when Vesta contained melt pockets in its mantle. Because this may cause differences in the heat budget of Vesta, we evaluated two endmember situations: A, where crust formation is instantaneous, and B, where crust formation does not take place at all. The actual situation for Vesta was probably somewhere between these two extremes. In endmember A, all the silicate melt migrates instantaneously to the surface, forming a magma body 2 Myr after core formation. (This is different from a magma ocean as hypothesized for example, by Righter and Drake (1997), where greater than 50% partial melting of the mantle takes place. In endmember A, this simplification is used because the rate and process of melt migration are not clearly understood). The choice of this time interval is such that silicate melting takes place at depths >15 km and the maximum temperature of the erupted Al-rich magma ocean does not exceed 1600 K. It should be mentioned that heat loss by convection is not considered in endmember A. Incorporation of this complexity would, of course, hasten the process of asteroidal cooling. In endmember B, the silicate melt does not migrate to form a crust but solidifies *in situ* in the mantle.

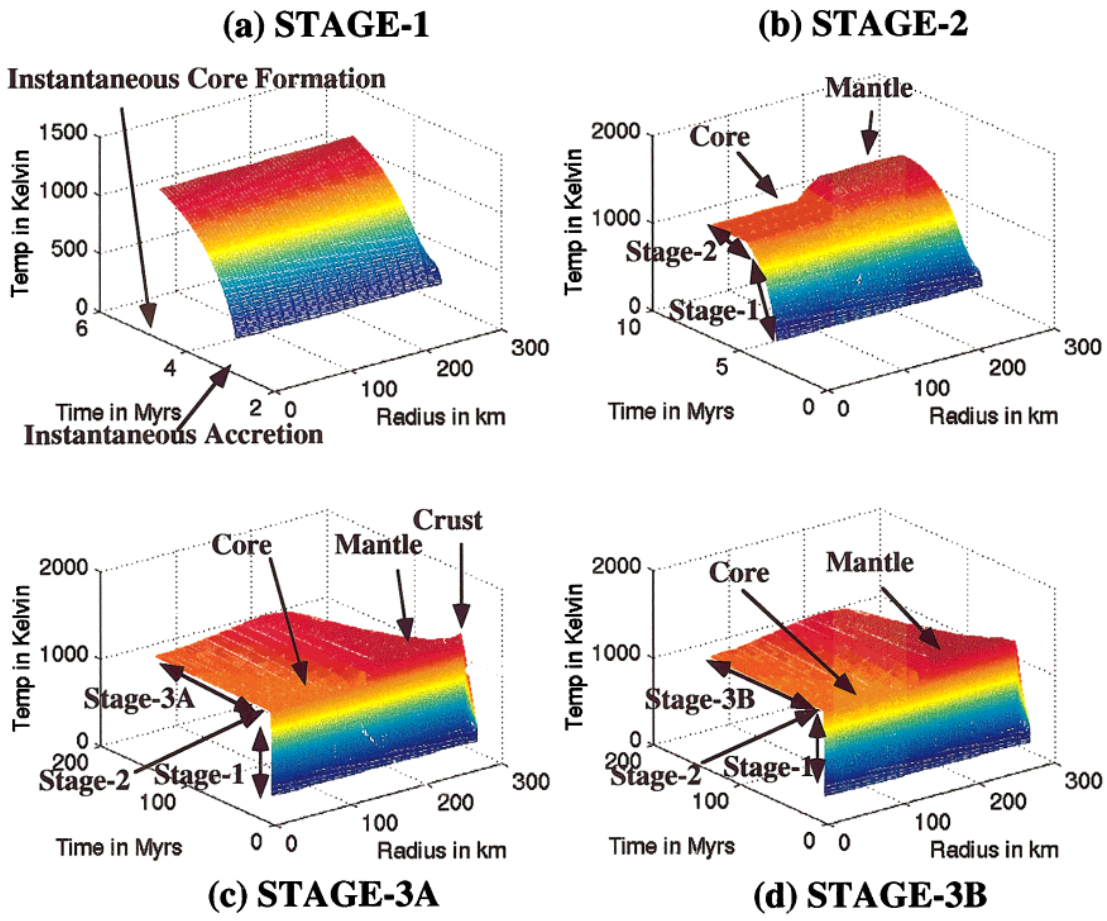

FIG. 3. Time–radius–temperature profiles of Vesta using a precursor composition of H-chondrite at the end of (a) stage 1, (b) stage 2, (c) stage 3, endmember A, and (d) stage 3, endmember B, respectively. Vesta undergoes heating from the temperature of the ambient nebula until iron-sulfide melting is completed (a). Instantaneous core separation marks the transition from stage 1 to stage 2, so that in stage 2, Vesta is no longer homogeneous but is composed of a core and mantle. Core formation results in redistribution of ^{26}Al, which causes the heat generation in the core to stop as observed by a thermal plateau at radii <110 km. Stage 2 ends after 25% partial melting of the mantle is attained. After stage 2, we evaluate two possibilities: (c) stage 3, endmember A, and (d) stage 3, endmember B. In (c), the silicate melt erupts instantaneously to form an eucritic crust, whereas in (d) the magma is assumed to solidify as intrusive dikes and plutons without erupting to the surface. In (c), Vesta is composed of a eucritic crust, an olivine mantle, and an Fe–FeS core. Redistribution of ^{26}Al causes a fourfold increase (compared to the source region) of ^{26}Al resulting in high crustal temperatures discernable in (c) as a spike at a radius of ~270 km about ~7 Myr after CAI formation. In contrast, there is no crust formation in (d), and consequently no near-surface temperature spike caused by migration of Al into eucritic crust. However, endmember-B is a more effective configuration when it comes to conservation of heat as compared to endmember A.

Stage 3: Subsequent Heating and Cooling of the Differentiated Asteroid

Endmember A: All melt extrudes. When the mantle reaches 1463 K, all magma is assumed to ascend instantaneously and extrude to form a eucritic crust. In effect, this forms a magma ocean, equal in thickness to the present crust of Vesta (although this ''magma body'' is of considerably less thickness than that envisioned in most magma ocean scenarios (e.g., Righter and Drake 1997, Ruzicka *et al.* 1996). The barren mantle and the core do not contain ^{26}Al. This causes heating in the mantle to stop, as shown by the thermal plateau in Fig. 3c. Notice that the time–temperature–radius surface becomes parallel to the *XY* plane after ~6 Myr, for radii between ~100 and 240 km in Fig. 3c. This thermal plateau lies at a higher temperature than the thermal plateau generated in the core, at a radius of <100 km. The crust, however, has undergone a fourfold enrichment of ^{26}Al compared with the abundance of ^{26}Al in the precursor mantle. Increase in ^{26}Al abundance produces renewed heating in the crust that causes the magma ocean to boil, and temperatures can reach 1600 K or more. Significantly, this renewed phase of heating causes another reverse thermal gradient that cuts off heat loss not only from the mantle and the core but also contributes some heat to the part of the mantle in contact with the

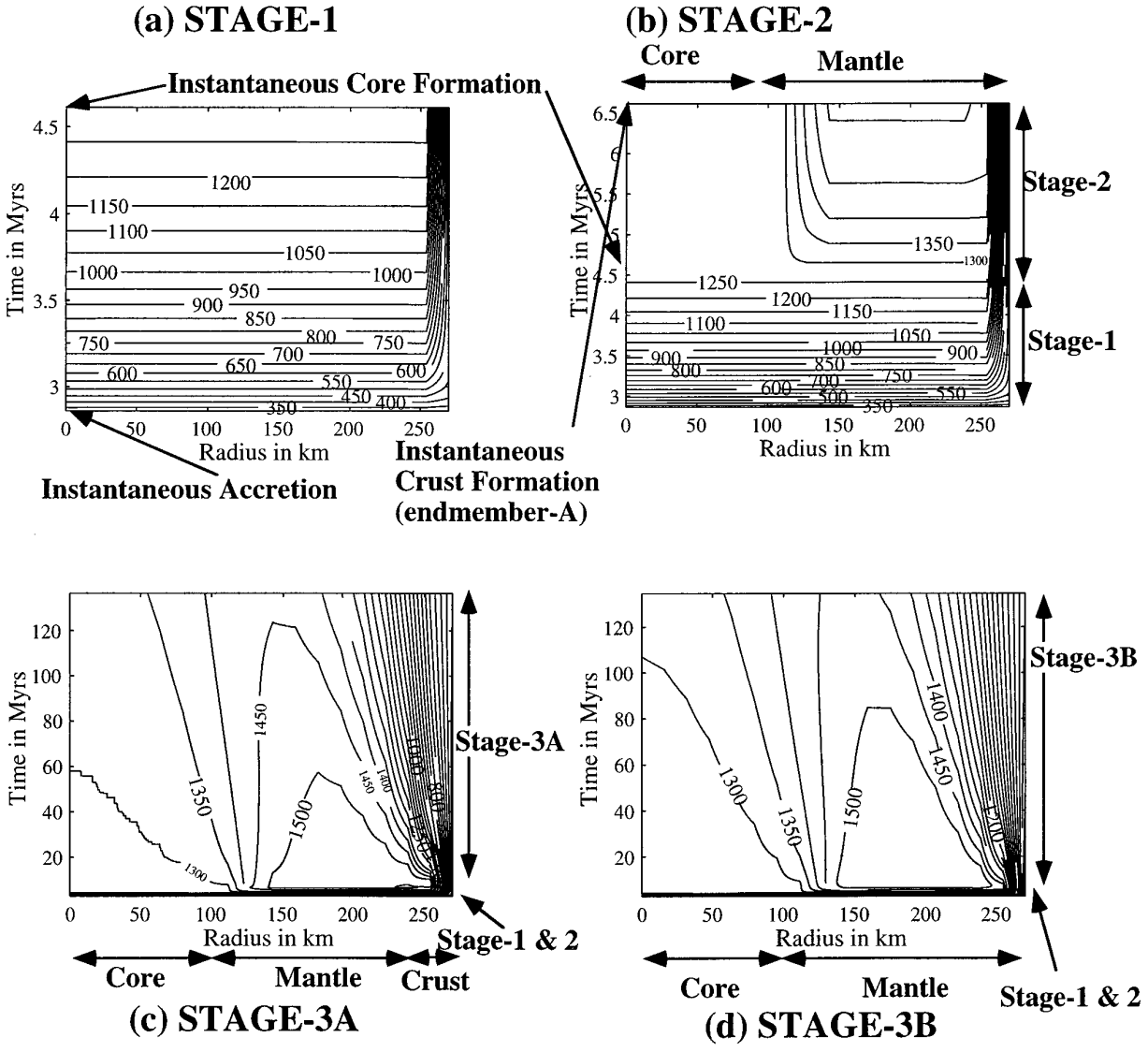

FIG. 4. Temperature (in Kelvin) contour plots of Vesta using a precursor composition of H-chondrite at the end of (a) stage 1, (b) stage 2, (c) stage 3, endmember A, and (d) stage 3, endmember B, respectively. (The corresponding 3D time–temperature–radius plots are given in Fig. 3). In stage 2, core formation results in redistribution of ^{26}Al, causing heat generation in the core to stop. This is clear after 4.58 Myr in (b) where high-temperature contours are seen in the mantle of Vesta, whereas the temperature of the core remains <1300 K. A comparison of the contour distributions in (c) and (d) reveals an essential difference in heat transfer between a configuration where the entire melt generated is extruded to near-surface layers (c) and one where the magma solidifies as plutons and intrusive dikes without eruption (d). Note that the high-temperature contours (e.g., 1450 K and 1500 K) are prevalent for longer periods of time in (d) than in (c). Also, note that heating of the core by conduction of heat from the overlying mantle is more profound in (d) because the mantle stays hotter in (d) than in (c).

crust. The reverse gradient dissolves ~13 Myr after CAI formation, so that heat loss from the mantle is revived. The fourfold Al enrichment of the crust relative to the mantle will cause uneven rates of heat generation which would maintain the reverse thermal gradient at least until the first 10 Myr (when heat generation of the crust with an Al abundance of 6.68% is considerable) relative to CAI formation.

Endmember B: No melt extrudes. In this scenario, it is assumed that eucritic magma does not migrate to the surface but solidifies within the mantle as plutons when the body cools. No perceptible difference between the thermal profiles for endmembers A and B is observed in Figs. 3c and 3d from the perspective of the 3D graph shown. Upon rotating the view by 180°, a small temperature spike is noticed at a radius of 250 km and at a time of 6 Myr in

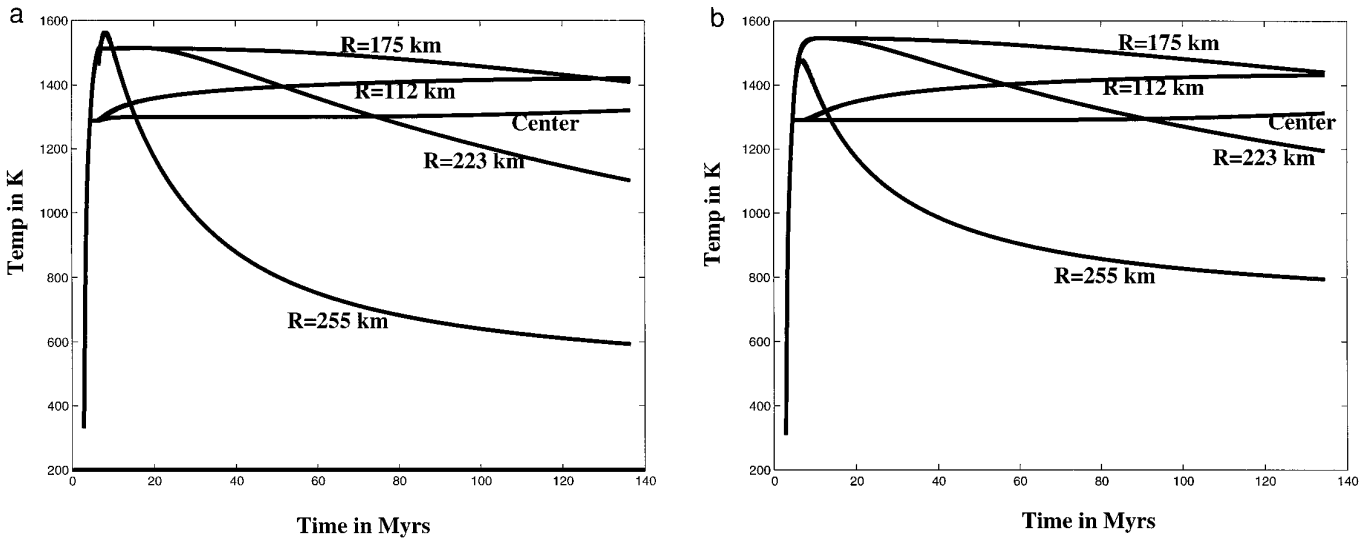

FIG. 5. Temperature–time history of Vesta at various depths for (a) endmember A and (b) endmember B. Note that after ~50 Myr, higher temperatures are observed in (b) than in (a). This happens because in (a) the heat source (^{26}Al) is brought closer to near-surface layers which are more susceptible to heat loss by radiation. In (b), the heat source stays buried in the interior, which results in a slower rate of heat loss from the asteroid.

Fig. 3c in contrast to Fig. 3d, where this temperature spike is not observed. Corresponding temperature–time plots are given in Figs. 5a and 5b, and temperature–depth plots for endmembers A and B are compared in Figs. 6a and 6b, respectively. Endmember B is used to rationalize the assumption of instantaneous crust formation and to test what effect magma movement has on thermal evolution. It should be noted that instantaneous crust formation does not technically happen in endmember B, because a crust does not form in this situation. In contrast to endmember A, no reverse thermal gradient is produced in the crust.

Neither of the two endmembers is likely to have happened. All the silicate melt probably did not migrate to form the crust instantaneously, and neither did it resolidify *in situ*. The reality is probably something between these two extremes—some of the melt might have crystallized as plutons and some may have percolated through the mantle and reached the surface. L. L. Wilson (pers. commun. 1996) calculated the time required for crust formation on Vesta to have been ~1 Myr; consequently, the assumption of instantaneous crust formation in endmember A will result in an error over about 1% of the entire time domain of this simulation (which runs for 130 Myr). The calculated temperature profiles for endmember B are different because a reverse thermal gradient does not form in the crust, as in endmember A.

A comparison of the contour plots in Figs. 4c and 4d shows that at ~100 Myr, the temperatures in the mantle and the crust in endmember B are higher than the corresponding temperatures at the same depths and times in endmember A. For example, the temperatures after 130 Myr at radii of 255, 223, and 175 km are lower in endmember A (Figs. 4c and 5a) compared to endmember B (Figs. 4d and 5b). This shows that the cooling time in endmember B is prolonged. In endmember A, a reverse thermal gradient exists in the crust–mantle boundary which insulates the interior from heat loss, extending the cooling time. Conversely, in endmember A, more of the heat source (^{26}Al) is incorporated in near-surface layers, which are susceptible to heat loss by radiation. This factor should decrease the time required for the body to cool. It is observed that cooling time in endmember A is shorter, so the second factor takes precedence over the first in controlling the cooling history. Thus, the eruption of basaltic magma on the surface of Vesta results in transfer of the heat source to the surface, which decreases the time interval over which the mantle and the core remain hot. The greater the amount of volcanism, the lower will be the retention of heat by the asteroid. The existence of a thick crust on Vesta would thus indicate a faster cooling time, whereas a thin crust with many plutons stranded in the mantle or in an unmelted carapace would point to a prolonged cooling history. We reiterate that heat loss by convection is not considered in endmember A and incorporation of this complexity will hasten the process of cooling.

DISCUSSION

Chronology

Accretionary time scale. In this model, accretion of Vesta was complete 2.85 ± 0.05 Myr after CAI formation.

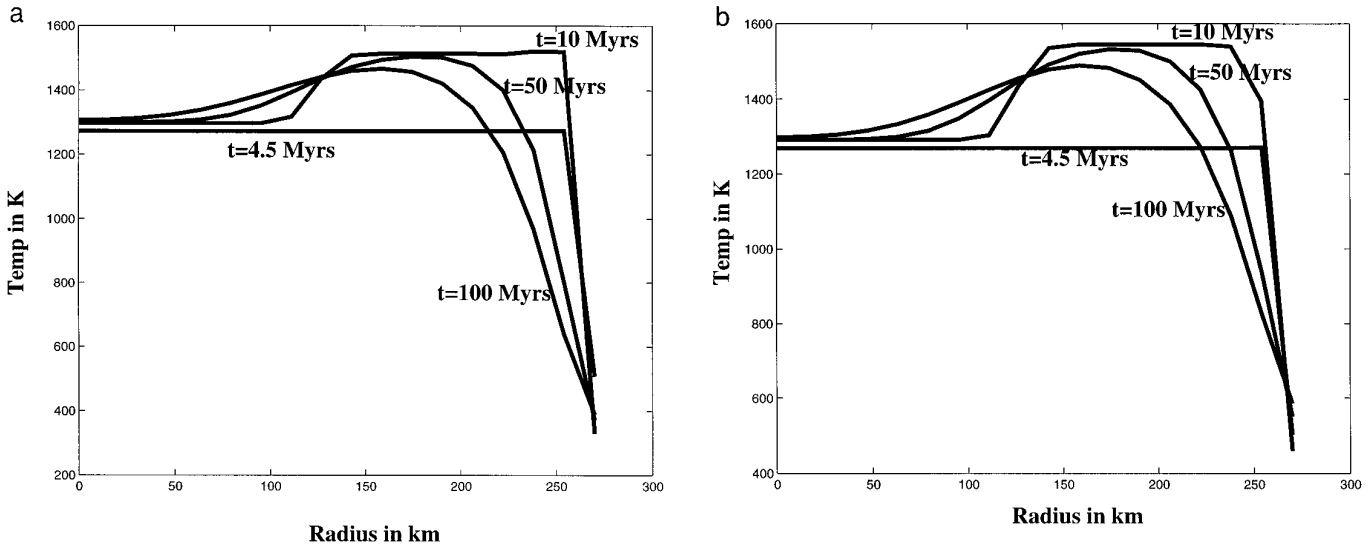

FIG. 6. Temperature–depth profiles at various times for (a) endmember A and (b) endmember B. Note the temperature spike caused by crust formation (and the associated migration of ^{26}Al) at 10 Myr at a radius of ~255 km for (a), which is absent in (b).

This result holds irrespective of the physics of the accretionary process. This bracketing of accretion time results from incorporation of the requisite amount of ^{26}Al to supply the necessary heat to cause 25% partial melting of Vesta's mantle. If the accretion time was earlier than 2.80 Myr, whole-mantle melting below a depth of 30 km would have taken place. Since evidence from HEDs suggests that eucrites were generated by not more than 25% partial melting of the source region (Stolper 1977, Jones *et al.* 1996), a lower limit for the accretion time of Vesta can be bracketed at 2.80 Myr. If the accretion time was later than 2.90 Myr, core formation does not take place in the model. If the accretion time was greater than 3.0 Myr, no melting of any kind occurs.

Iron-sulfide partial melting. The time of core formation according to the simulation is 4.58 ± 0.05 Myr after CAI formation, assuming that core formation predated igneous activity (Hewins and Newsom 1988) and that metal separation from the silicate matrix took place without the initiation of silicate melting. If core formation was contemporaneous with igneous activity, 4.58 Myr corresponds approximately to the time of initiation of eutectic Fe–FeS melting.

High resolution ^{53}Mn–^{53}Cr chronology of the Juvinas and Chervony Kut eucrites yields an age of 4565 ± 1 Ma (Shokolyukov and Lugmair 1997) for HED mantle fractionation. Pb isotope chronometry data (Gopel *et al.* 1991) place CAI formation at 4566 ± 2 Ma. This yields a time of 1 Ma (±3 Ma) for metal sulfide melting on the HED parent body, relative to CAI formation (G. Lugmair, pers. commun. 1997). ^{182}Hf–^{182}W chronology (Lee and Halliday 1997) of two eucrites (Juvinas and ALHA 78192) yields ages of metal segregation between 4 and 15 Myr relative to CAI formation. Our calculated time of core formation appears to be in acceptable agreement with high-resolution chronological data.

Silicate partial melting. The melting temperature for eucritic liquids is reached at 6.58 ± 0.05 Myr after CAI formation. This corresponds approximately to the lower limit of the ages of noncumulate eucrites. For volcanism to take place before 6.58 ± 0.05 Myr, the accretion time would have to be less than 2.85 ± 0.05 Myr, which will in turn cause >25% partial melting on Vesta. Initial Sr isotopic evolution suggests an age of 8.8 Myr (relative to CAIs) for noncumulate eucrites (Podosek and Cassen 1994) corresponding to the time of silicate melting on the HED parent body.

The most stringent limit on initial ^{26}Al/^{27}Al ratios in eucrite magmas, based on measurements of Moore County, is $<5 \times 10^{-8}$(Schramm *et al.* 1970), in good agreement with the ratio expected from our model. The first-formed volcanic rocks on Vesta, according to our thermal model, would show a ^{26}Al/^{27}Al ratio $<9.6 \times 10^{-8}$. The absence of ^{26}Al in noncumulate eucrites like Juvinas and Pasamonte has been cited previously as evidence indicating that ^{26}Al was not the heat source (Wood and Pellas 1991). The simulation shows that if ^{26}Al was the heat source, the time of volcanism was such that the ^{26}Al content of eucrites would have fallen below detectable limits.

The heat source has to lose its efficacy after 25% partial melting of the mantle is accomplished. If it does not, whole-mantle melting takes place on Vesta, which is incompatible with most current ideas of the petrogenesis of HEDs. Thus, igneous activity which produced the first-formed volcanic

rocks on Vesta took place at a time when the heat source had started to lose its potency: thus, it is not surprising that noncumulate eucrites did not contain enough ^{26}Al to cause heating. Self-diffusion of Mg in plagioclase may cause post-crystallization redistribution of ^{26}Mg (LaTourrette and Wasserburg 1997). This explanation, though possible, may not be necessary (because the ^{26}Al abundance at the time of eruption of noncumulate eucrites is already low).

Cooling until geochemical closure. Because of a prolonged cooling history, it is possible to sustain volcanism on Vesta for at least 100 Myr using short-lived radionuclides as heat sources, even though ^{26}Al loses its potency with a few million years after the accretion of Vesta. Time-temperature profiles and time-depth profiles (Figs. 5 and 6) for endmembers A and B show that a considerable portion of Vesta's interior is maintained at >1400 K after 100 Ma. For example, temperatures at a depth of 95 km could stay high enough to prevent isotopic closure and even sustain a magma chamber, which could erupt after 100 Myr to produce cumulate eucrites. (It is not implied that magma *generation* occurred after 100 Myr. This can happen, as argued below, only between 5.5 and 8 Myr. Neither are we advocating that a magma eruption is necessary to generate eucrites. Chronometers in cumulate eucrites possibly record isotopic closure, not necessarily igneous crystallization.)

The prolonged cooling history can be attributed to three factors: the reverse thermal gradient in the core after metal segregration, the reverse thermal gradient in the crust after crust formation, and the low thermal diffusivity of silicates. The prolonged cooling history of Vesta does away with a scenario where melt stored in a magma chamber for 100 Myr (Haack *et al.* 1990) erupts suddenly by impact (Taylor 1988) to produce cumulate eucrites. Consideration of a megaregolith on Vesta (e.g., Haack *et al.* 1990) would cause a slower rate of cooling on Vesta. This would cause the mantle of Vesta to stay hot enough to prevent geochemical closure even longer than the present model.

Comparison of Thermal Histories for H, L, and LL Chondrite Bulk Compositions

Differences in the bulk composition control the size of the core and the Al abundance per unit mass (which affects ^{26}Al per unit mass). In our simulation, we observe the following variations due to change in bulk composition from H to L to LL chondrite: the size of the core decreases from 123 to 108 to 92 km, and the thickness of the crust increases from 27.2 to 28.2 to 29.1 km. The accretion time for 25% partial melting decreases slightly from 2.85 to 2.80 to 2.75 Myr due to increase in Al abundance per unit mass, and the time required for core formation also decreases from 4.58 to 4.42 to 4.28 Myr for the same reason.

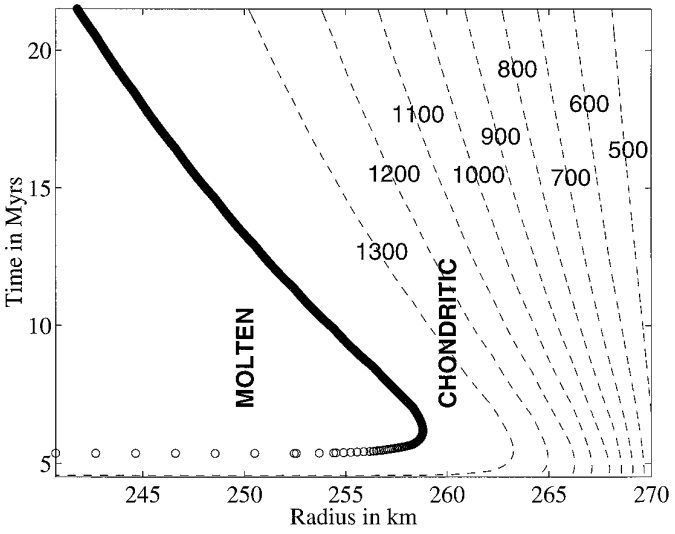

FIG. 7. Temperature evolution in the crust and upper mantle of Vesta until 10 Myr after CAI formation. The contour interval is 50 K for temperatures >1200 K and 100 K for temperatures <1200 K. This is evaluated for endmember B, i.e., an assumption is made that the magma does not migrate after partial melting. Note that a shell of 15 km thickness does not attain temperatures capable of initiating silicate partial melting. For extrusive volcanism to take place, the magma has to percolate through the chondritic surface layer in order to erupt. The process of percolation of a Al-rich melt through the chondritic carapace is expected to cause melting and metamorphism, but will this cause the carapace to disintegrate? The carapace might survive at low degrees of partial melting but will probably become vulnerable to destruction at higher degrees of partial melting.

Survival of Precursor Materials on Vesta

The thermal model suggests the possibility that chondritic rocks in the outer layers of Vesta before crust formation may still exist. Though this idea is radical, it is difficult to rationalize why this would not happen. The outer carapace never experiences high temperatures. In fact, this is why a ''trigger'' at a depth of 30 km is used to initiate core formation. No matter how great the abundance of ^{26}Al, the near-surface layers never experience temperatures close to silicate or sulfide melting if a radiation boundary condition is maintained at the surface. This can be illustrated from the results of endmember B, where crust formation does not take place. Notice that in Fig. 7 the high-temperature contours never extend to the surface or near-surface layers. According to this figure, an outer shell ~10 km would undergo neither silicate nor sulfide melting, although parts of it may be metamorphosed. Figure 6b shows that at 10 Myr, the temperature of the surface is ~500 K, and the temperature at a depth of 25 km approaches the temperature of the silicate solidus. The contour plot of temperature (Fig. 7) shows that neither the 1200 K nor the 1400 K contours touch the right margin of the plot corresponding to a radius of 270 km. In fact, according to Fig. 7, a layer

more than 10 km in thickness should not melt on Vesta. Figure 5a shows evolution of temperature with time at 15 km depth (i.e., at a radius of 255 km). Note that at this depth, the peak temperature barely reaches the temperature of silicate melting.

Could impacts destroy a 10-km-thick carapace? Small impacts are apparently not capable of causing widespread melting (Keil *et al*. 1996, Melosh 1990) but large impacts are capable of producing widespread melting and disruption. Even in this case, however, the melting will not be global, being more pronounced in the hemisphere affected by the impact and leaving the other hemisphere unaltered or metamorphosed (Williams and Wetherill 1993).

Eucrites that erupt on Vesta must percolate through this thick carapace to erupt on the surface. The carapace may partially melt during the intrusion of the ^{26}Al-rich eucritic dikes. Indeed, the distribution of these dikes determines whether the carapace can survive without melting. It is possible that part of the chondritic precursor material of Vesta survives as metamorphosed chondrite, either as a near-surface layer or in screens between plutons. Although we are unaware of any descriptions of metamorphosed chondritic xenoliths in eucrites (though carbonaceous chondritic clasts do occur in howardite regolith breccias (Zolensky *et al*. 1996), thermal considerations might suggest that some precursor material may have survived the vigorous heating event on Vesta. It is conceivable that some craters on Vesta (Gaffey 1997, Thomas *et al*. 1997a) may not have exposed mantle, but a remnant portion of the outer layer of proto-Vesta which survived the asteroid's differentiation. This might produce a unique stratigraphy on Vesta with the following sequence from the top to the bottom: eucritic lava flows, metamorphosed chondrite interspersed with eucritic dikes or plutonic rocks (which do not penetrate the carapace), and depleted mantle from which the eucritic lava originated.

If indeed, precursor material were to be found on Vesta, then a host of interesting possibilities arise. For example, silicate melting may have been a far more common occurrence in the early Solar System, but in most asteroids the silicate melt may not have been able to percolate through the unmelted carapace to erupt on the surface. Thus, the apparent absence of basaltic surfaces on asteroids does not obviate the possibility of differentiation; rather a core, mantle, and igneous plutons may lie beneath an unmelted chondritic veneer.

Effectiveness of ^{60}Fe as a Heat Source

The rate of heat generation per kilogram due to decay of ^{26}Al is three to four orders of magnitude greater than that of ^{60}Fe. The local abundance of ^{60}Fe increases four times when Fe is segregated into the core during core formation, but this is hardly sufficient to offset a difference of four orders of magnitude. Thus, given an initial ratio of ^{60}Fe/^{56}Fe equal to 2×10^{-8} (Shukolyukov and Lugmair 1997), ^{60}Fe decay fails to make a perceptible difference in the thermal history, even when it is concentrated during core segregration.

V. SUMMARY AND CONCLUSIONS

The assumptions and uncertainties in the thermal model are as follows:

(i) It is assumed that the ratio of ^{26}Al/^{27}Al at the time of CAI formation was 5×10^{-5} and that its distribution in the nebula was homogeneous at least on the scale of materials coaccreted to form planetesimals.

(ii) Vesta is assumed to be the parent body of HED meteorites, so that chronological and geochemical constraints from these samples apply to Vesta.

(iii) The ambient temperature at the heliocentric location of Vesta is evaluated by recalculating the solar constant assuming condensation of ice outboard of 2.7 AU, and is assumed to stay constant with time.

(iv) Assumptions were made to offset the following uncertainties:

(a) The composition and the size of the core are not known.

(b) The bulk composition of Vesta is uncertain.

(c) It is not known whether core formation in Vesta predated igneous activity, whether it was nearly instantaneous, and at what temperature metal segregation took place.

(d) The proportion of the silicate melt that could percolate through the ''frozen'' layer, the proportion that solidifies as plutons in the ''frozen'' layer, and the proportion that solidifies in the mantle are not known.

(e) The amount of partial melting on Vesta is unknown: Experimental work suggests that 25% partial melting produced the noncumulate eucrite Sioux County (Jones *et al*. 1996).

The simulation of the thermal history of Vesta indicates that in order to achieve 25% partial melting on Vesta by ^{26}Al decay, accretion had to end at 2.85 ± 0.05 Myr after CAI formation. Core formation occurred at 4.58 ± 0.05 Myr and crust formation at 6.58 ± 0.05 Myr. The age of crust formation explains why noncumulate eucrites should not record detectable ^{26}Mg excesses, a major problem cited against the hypothesis of heating by ^{26}Al (Wood and Pellas 1991). Geochemical closure at a depth of $\geq$100 km or more on Vesta is not attained until 100 Myr, which could explain a time interval of 100 Myr between cumulate and noncumulate eucrites. This observation shows that it is possible to sustain heat generated by ^{26}Al decay for a longer time than previously estimated and solves another problem

raised about the ^{26}Al heating hypothesis. The thermal model argues for the possible preservation of primitive near-surface material on Vesta, which escaped melting and differentiation. The effect of ^{60}Fe as a heat source is found to be negligible.

APPENDIX: GOVERNING EQUATION AND MODEL PARAMETERS

The relation

$$\frac{\partial T}{\partial t} = \frac{1}{R^2}\frac{d}{dR}\left(R^2\kappa\frac{\partial T}{\partial R}\right) + \frac{Q_{\text{radnl}}}{\rho c_v}$$

is the fundamental heat transfer equation where T is temperature, R radius of the asteroid, t time, κ thermal diffusivity, Q_{radnl} heat generated by radioactive decay, ρ density, and c_v specific heat at constant volume. To appreciate the subtleties of the model, it is useful to understand how each term in the equation might affect the solution. The term on the left side is the rate of change of temperature (T) with time (t) in a layer of infinitesimal thickness at any arbitrary depth in the asteroid. The first term on the right side of the equation gives the amount of heat gained in (or lost by) the infinitesimal layer from the surrounding layers by conduction and is known as the conduction or diffusion term. In words, it means that the amount of heat transmitted in this fashion is proportional to the rate at which the product of thermal gradient ($\delta T/\delta R$) and thermal diffusivity (κ) changes. Thermal diffusivities of rocks are typically low (around 10^{-7} m^2 s^{-1}) and are functions of temperature. The thermal diffusivities, as a function of temperature, for various rock types are taken from Yomogida and Matsui (1983).

The last term on the right side gives the amount of heat that is generated in the asteroid. Q_{radnl} varies with the live ^{26}Al and ^{60}Fe present and the absolute abundance of Al and Fe. It can be represented mathematically as:

$$Q_{\text{radnl}} = A_{0\text{Al}}Q_{0\text{Al}}e^{-\lambda_{\text{Al}}t} + A_{0\text{Fe}}Q_{0\text{Fe}}e^{-\lambda_{\text{Fe}}t},$$

where A_0 is initial abundance, Q_0 initial heat production per unit volume, and λ decay constant.

1.1. Numerical Method and Algorithm Development

This is the first attempt at modeling the thermal history of a differentiated asteroid, through core and crust formation and cooling. The Dirichlet boundary condition, an approximation that fixes the temperature of the surface to be equal to the ambient nebular temperature, has been used in past asteroid thermal models, in contrast to the radiation boundary condition used here, which involves much greater numerical instability. This is also the first finite element model of an asteroid. The finite element method uses a basis function to minimize approximation error during numerical integration, and has been found to be more accurate than the finite difference method or the classical series solution (Baker and Pepper 1991).

The mode of derivation of the Galerkin Weak Statement (and the subsequent matrix form of the equation) from the heat transfer equation is after Baker and Pepper (1991). The temperature is approximated by a trial function which does not coincide with the exact solution of the differential equation for a particular value of the spatial dimension, r. Hence,

$$T(r) = T^N(r) + e^N(r),$$

where $T(r)$ is the exact solution, $T^N(r)$ is the numerical approximation, and $e^N(r)$ is the error. One of the primary concerns of a simulation is to minimize the approximation error $e^N(r)$. An estimate of the error can be found by substituting it in the differential equation, ($L(T) = 0$) to be solved.

Thus, $L(e^N) = L(T) - L(T^N)$.

Since, $L(T) = 0$, $L(e^N) = -L(T^N)$.

Thus, the trial function, when substituted in the differential equation, does not equal zero, as required by the differential equation. This cannot be done because forcing $L(T^N)$ to be equal to zero amounts to evaluating the exact solution. Instead, a rational approach is to make a measure of approximation error disappear in the overall integrated sense over the domain. This is done by setting the weighted residuals to go to zero over the entire domain as represented by the following mathematical statement:

$$\int_\Omega w_i(x)L(T^N)\,dx \equiv 0, \qquad \text{for } 1 \le i \le N.$$

The weight function w_i is made identical to the trial function. This is called the Galerkin criteria which ensures the minimization of approximation error since it is orthogonal (in the mathematical sense means that the distance between the curves of the exact solution and the approximation is minimum) to the trial function. After implementing the weak statement, first-order Lagrange interpolation polynomials are chosen as the trial functions. Subsequently the trial function is written as a basis function for each generic finite element. The matrix statement is written and the boundary conditions are implemented at the two boundaries of the linear domain. Since a sphere is symmetric about a radius (and considering the fact that the asteroid does not have any directional heterogeneity in thermal properties), the formulation of the heat transfer equation in polar coordinates makes the problem one-dimensional. A time Taylor series is written on the matrix statement and the trapezoidal rule is implemented.

The asteroid goes through a complex history of melting, differentiation, and cooling. To implement the complex evolution, the code has been divided into three time domains corresponding to the three stages in Table I. The values of thermal diffusivity and specific heat are updated (as a function of temperature) for each time step.

Numerical accuracy and convergence analysis were performed for progressively coarse meshes to determine an adequate mesh size. The numerical error can be written as

$$T^h + e^h = T_{\text{exact}} = T^{h/2} + e^{h/2},$$

where T^h and $T^{h/2}$ are the solutions for a particular mesh size and its double mesh refinement, respectively, e^h and $e^{h/2}$ the errors for a particular mesh size and its double mesh refinement, respectively, and T_{exact} the exact solution.

Approximation error has the following functional form (Baker and Pepper 1991):

$$e^h = C_k l_e 2k.$$

Therefore, the relation between T^h and $T^{h/2}$ can be written as follows:

$$T^h - T^{h/2} = (2^{2k} - 1)e^h.$$

Assuming $\Delta T^{h/2} = T^h - T^{h/2}$, the error in the finer grid solution can be written as

$$e^{h/2} = \Delta T^{h/2}/(2^{2k} - 1).$$

The slope of a log–log plot of numerical error and length of a finite element (l_e)would be expressed as

$$\text{slope} = [\log(e^{h/M}) - \log(e^{h/2M})]/[(\log(l_e) - \log(l_{e/2}))].$$

TABLE A1
Verification of Numerical Error by Adjusting the Coarseness of the Mesh

No. of finite elements	Temperature	Estimated error	Estimated T (exact)	Slope
15	946.40			
30	940.57	1.94	938.63	
60	939.16	0.47	938.69	2.05

For ideal convergence, the above expression should theoretically be equal to 2 for a linear basis ($k = 1$) approximation. Progressive mesh refinements were performed and the value of slope was found to equal to 2.05 (see Table A1).

In stage 1, there is one macrodomain composed of precursor material. In stage 2, the asteroid has two macrodomains—an inner core and an outer mantle. In stage 3, the asteroid has three macrodomains—an inner core, an intervening mantle, and an outer crust (see Table A2). For each material type, the corresponding specific heat capacities and thermal diffusivities are calculated. The heat generated per unit time in a macrodomain is dependent on the Al abundance and the amount of live ^{26}Al present, and is computed depending on the type of material present in a macrodomain.

1.2. Specific Heat Capacity

Specific heat capacity at constant pressure (c_p) is converted to specific heat at constant volume (c_v) using the relation (Navrotsky 1994)

$$c_p - c_v = \frac{TV\alpha^2}{\beta},$$

where T is temperature, V volume, α thermal expansivity, and β compressibility or reciprocal of bulk modulus. Since it is observed that c_p and c_v values closely match (the difference being at most a few percent at higher temperatures), this calculation is approximated for the whole rock using one (very abundant) mineral—olivine. Substituting actual values for other minerals is expected to yield little difference from this simplification.

Net specific heat is calculated as

$$c_v = \frac{\sum_{n=1}^{k} c_v^k m_k}{\sum_{n=1}^{k} m_k},$$

where c_v^k is the specific heat of the kth mineral, and m_k weight fraction of the kth mineral. Specific heat capacity is dependent on temperature. Experimental data from Robie *et al.* (1977) have been used to take this into account.

Most previous thermal models (e.g., Miyamoto *et al.* 1981, Grimm and McSween 1989) have used c_p. Because the temperature rise is caused by a change in the internal energy, c_v should be used (for a detailed formulation, see White 1985). However, the difference in c_p and c_v for solids is negligible and yields little difference in thermal histories.

1.3. Boundary Condition

The heat flux at the center of the asteroid is assumed to be zero. The heat loss from the surface of the asteroid is governed by the radiation boundary condition and given by

$$\left.\frac{dT}{dR}\right|_{R=R'} = \frac{e\sigma}{k}(T_{surf}^4 - T_{neb}^4),$$

where R' is the radius at the surface, T_{surf} temperature at the surface of the asteroid, T_{neb} temperature of the surrounding nebula, e emissivity, and σ Stefan Boltzmann constant. T_{neb} is assumed to be the same as the initial temperature throughout the time domain. There is no rationale for this assumption, except that the rate of decrease of temperature with time at a particular heliocentric distance is as yet an unsolved problem (A. Boss, pers. commun., 1996).

Grimm and McSween (1989), Miyamoto *et al.* (1981), etc., use a Dirichlet boundary condition according to which the temperature at the surface of the asteroid is set to be the same as the temperature of the surroundings. This is a valid assumption if the range of peak temperatures attained in the asteroid is close to the ambient temperature. The greater the difference between peak temperature and nebular temperature, the greater will be the error when a Dirichlet boundary condition is used. This happens because in order to make the temperature on the surface of the asteroid equal to the temperature of the surrounding nebula, a higher heat flux than is allowed by the radiation boundary condition (which represents the actual physical constraint for heat transfer at the surface of the asteroid) must be invoked. A Dirichlet boundary condition will result in lower peak temperatures and higher cooling rates.

1.4. Effect of Emissivity

A change in emissivity by an order of magnitude does not significantly alter the peak temperature or the cooling profile. This is because a negative feedback mechanism causes the heat flux from the asteroid to stabilize at a certain level for a particular temperature, irrespective of emissivity. A decrease in emissivity keeps the surface temperature high, which, in turn, causes the temperature difference between the surface and the surroundings to increase. This results in a greater heat flux and a decrease in temperature, thereby offsetting the temperature increase caused by a decrease in emissivity.

1.5. Dependence of Thermal Model on Variable Parameters: A Summary

This section assumes that the constraint of 25% partial melting on the HED partial melting (Jones 1984) is met by our thermal model. An increase of either the initial abundance of 26Al or the abundance of 26Al per unit mass by 100% causes the entire chronology (time of accretion,

TABLE A2
Finite Element Domain Discretization in Spatial and Temporal Domains

	Spatial domain		Time domain	
	No. of nodes	Mesh progression ratio	No. of nodes	Mesh progression ratio
Stage 1	85	0.98	173	1
Stage 2 (core)			200	1
Core	30	1.01		
Mantle	60	1.005		
Stage 3			2700	1.002
Core	30	1.01		
Mantle	40	1.005		
Crust	20	1.001		

TABLE A3
Mineral Abundances (wt%), Abundance of Al and Fe (wt%), and Bulk Density (kg/m^3)

	Eucritic crust	Barren mantle	Fertile mantle	Core	H chondrite
Quartz	1.83	0.00	0.00	0.00	0.00
Orthoclase	0.24	0.00	0.24	0.00	0.53
Albite	3.98	0.00	3.81	0.00	7.27
Anorthite	33.25	0.00	6.81	0.00	1.70
Fayalite	0.00	25.27	45.32	0.00	6.29
Forsterite	0.00	74.73	33.82	0.00	25.99
Diopside	14.98	0.00	5.03	0.00	4.13
Hypersthene	44.77	0.00	5.16	0.00	19.33
Chromite	0.50	0.00	0.50	0.00	0.76
Ilmenite	1.20	0.00	0.30	0.00	0.23
Apatite	0.22	0.00	0.05	0.00	0.64
Fe (metal)	0.00	0.00	0.00	89.3	15.21
Ni	0.00	0.00	0.00	4.13	2.68
FeS	0.00	0.00	0.00	5.33	5.47
Bulk Al	6.68	0.00	1.69	0.00	1.33
Bulk Fe	14.62	21.23	0.00	89.34	15.21
Density (kg/m^3)	2700	3500	3500	7540	3500

time of core formation, and time of crust formation) of Vesta presented to move forward by 0.72 Myr. For example, the time of core formation becomes 4.58 + 0.72 Myr. Conversely, decreasing the parameters by 50% causes the entire chronology to be pushed back by 0.72 Myr. As discussed in the text, decreasing the initial temperature from 292 to 270 K causes the chronology to be pushed back by 0.09 Myr. Conversely, an increase in the initial temperature will cause the chronology to be pushed forward. A decrease in specific heat capacity will result in higher temperatures with the same amount of heat. This will cause the entire chronology to be moved forward. Similarly, higher specific heat capacities will cause the chronology to move back. A change in the bulk composition of Vesta changes the Al abundance per unit mass and the amount of metal. The change in bulk composition from H to L to LL chondrite causes the size of the core to decrease from 123 to 108 to 92 km and the time of accretion to decrease from 2.85 to 2.80 to 2.75 Myr (times of Fe–FeS and silicate partial melting also undergo a corresponding decrease). The 0.05 Myr error bar refers to the window in the chronology of Vesta which can reproduce the observation of 25% partial melting on Vesta (for detailed explanation, see section on Chronology, under Discussion).

1.6. Model Parameters

(See also Table A3.)
Heliocentric distance of Vesta = 2.36 AU
Initial temperature of Vesta = 292 K
Emissivity = 0.8
Albedo = 0.05
Radius of Vesta = 270 km
$^{26}Al/^{27}Al$ at time of CAI formation = 5×10^{-5}
$^{60}Fe/^{56}Fe$ at time of CAI formation = 1×10^{-8}
Liquidus:
  Fe–FeS system = 1233 K
  Eucritic basalt = 1463 K
Solidus:
  Fe–FeS system = 1213 K
  Eucritic basalt = 1443 K
Latent heat of melting:
  Iron = 271,000 J/kg
  Basalt = 400,000 J/kg
Discontinuities:
  Core–mantle transition = 123.41 km
  Crust–mantle transition = 242.75 km
Specific of liquids:
  Iron = 2000 J/kg/K
  Basalt = 2000 J/kg/K
  Thermal expansivity of olivine = 3.8×10^{-5}
  Compressibility (reciprocal of bulk modulus) of olivine = 1.82×10^{-6}
  Molar volume of olivine = 331.145
  Half life of ^{26}Al = 0.72 Myrs
  Half life of ^{60}Fe = 1.5 Myrs
  Decay energy of ^{26}Al = 3 MeV per atom
  Decay energy of ^{60}Fe = 3 MeV per atom
  Solar constant = 1360 W/m^2

ACKNOWLEDGMENTS

This work was supported by NASA Grant NAG 54387 and discretionary funds of the Department of Geological Sciences, University of Tennessee. A. J. Baker helped set up the problem in its finite element formulation. R. T. Williams and T. C. Labotka reviewed an earlier version of the manuscript. We thank C. Halloy, Director of Joint Institute for Computational Science at the University of Tennessee, for providing access to high-performance computers, Sun workstations, and color printers. We thank Marvin Bennett for his help with the figures. We also acknowledge H. Newsom and H. Haack for constructive reviews.

REFERENCES

Allegre, C. J., J. L. Birck, S. Fourcase, and M. Semet 1975. $^{87}Rb/^{87}Sr$ age of the Juvinas basaltic achondrite and early igneous activity of the Solar System. Science **187,** 346–348.

Baker, A. J., and D. W. Pepper 1991. *Finite Element 1–2–3,* McGraw-Hill, New York.

Barshay, S. S., and J. S. Lewis 1976. Chemistry of primitive solar material. *Annu. Rev. Astron. Astrophys.* **14,** 81–94.

Basaltic Volcanism Study Project 1981. *Basaltic Volcanism on the Terrestrial Planets*. Pergamon, New York.

Bell, J. F., D. R. Davis, W. K. Hartmann, and M. J. Gaffey 1989. Asteroids—The big picture. In *Asteroids-II*, pp. 921–945. Univ. of Arizona Press, Tucson.

Bennett, M. E., and H. Y. McSween, Jr. 1996. A revised thermal model for ordinary chondrite parent bodies. *Meteor. Planet. Sci.* **31,** 783–792.

Binzel, R. P., and S. Xu 1993. Chips off Asteroid 4 Vesta: Evidence for the parent body of basaltic achondrite meteorites. *Science* **260,** 186–191.

Binzel, R. P., M. J. Gaffey, P. C. Tomas, B. H. Zellner, A. D. Storrs, and E. N. Wells 1997. Geologic mapping of Vesta from 1994 Hubble Space Telescope images. *Icarus* **128,** 95–103.

Birck, J. L., and C. J. Allegre 1978. Chronology and chemical history of the basaltic achondrite parent body studied by $^{87}Rb/^{87}Sr$ method. *Earth Planet. Sci.* **39,** 37–51.

Boesenberg, J. S., and J. S. Delaney 1997. A model composition of the basaltic achondrite planetoid. *Geochim. Cosmochim. Acta* **61,** 3205–3225.

Bogard, D. D. 1995. Impact ages of meteorites: A synthesis. *Meteoritics* **30,** 244–268.

Boss, A. P. 1990. 3D solar nebula models. In *Origin of the Earth* (H. E. Newsom and J. H. Jones, Eds.), pp. 3–15. Oxford Univ. Press, New York.

Bunch, T. E. 1975. Petrography and petrology of basaltic achondrite polymict breccias howardites. *Proc. Lunar. Planet. Sci. Conf. 6th*, 469–493.

Cameron, A. G. W. 1962. The formation of the sun and planets. *Icarus* **1,** 13–69.

Cameron, A. G. W., and M. R. Pine 1973. Numerical models of the primitive solar nebula. *Icarus* **18,** 377–406.

Carlsson, R. W., F. Tera, and N. Z. Boctor 1988. Radiometric geochronology of the eucrites Nuevo Laredo and Bereba. *Lunar. Planet. Sci. Conf. 19th,* 166–167.

Clayton, R. N., and T. K. Mayeda 1983. Oxygen isotopes in eucrites, shergottites, nakhlites and chassignites. *Earth Planet. Sci. Lett.* **62,** 1–6.

Clayton, R. N. 1993. Oxygen isotopes in meteorites. *Annu. Rev. Earth Planet. Sci.* **21,** 115–149.

Consolmagno, G. J., and M. J. Drake 1977. Composition and evolution of the eucrite parent body: Evidence from rare earth elements. *Geochim. Cosmochim. Acta* **41,** 1271–1282.

Desnoyers, C., and D. Y. Jerome 1977. The Malvern howardite: A petrological and chemical discussion. *Geochim. Cosmochim. Acta* **41,** 81–86.

Drake, M. J. 1979. Geochemical evolution of the eucrite parent body: Possible nature and evolution of Asteroid 4 Vesta. In *Asteroids* (T. Gehrels and M. S. Matthews, Eds.), pp. 765–782. Univ. of Arizona Press, Tucson.

Driebus, G., J. Bruckner, and H. Wanke 1997. On the core mass of asteroid 4 Vesta. *Meteor. Planet. Sci.* **32,** A36.

Drummond, J., A. Eckart, and E. K. Hage 1988. Speckle interferometry of asteroids. IV. Reconstructed images of 4 Vesta. *Icarus* **73,** 1–14.

Duke, M. B., and L. T. Silver 1967. Petrology of eucrites, howardites and mesosiderites. *Geochim. Cosmochim. Acta* **31,** 1637–1665.

Dymek, R. G., A. L. Albee, A. A. Chodos, and G. J. Wasserburg 1976. Petrography of isotopically dated clasts in the Kapoeta howardite and petrologic constraints on the evolution of its parent body. *Geochim. Cosmochim. Acta* **40,** 1115–30.

Edwards, S., S. Cabrit, L. O. Ghandour, and S. E. Strom 1989. Forbidden lines in the T-Tauri star spectra: A clue to the origin of T-Tauri winds. In *ESO workshop on Low Mass Star Formation and Pre Main Sequence Objects* (B. Reipurth, Ed.), pp. 385–397. European Southern Observatory, Garching.

Farinella, P., R. Gonczi, C. Froeschle, and C. Froeschle 1993. The injection of asteroid fragments into resonances. *Icarus* **101,** 174–187.

Gaffey, M. J. 1997. Surface lithologic heterogeneity of Asteroid 4 Vesta. *Icarus* **127,** 130–157.

Ghosh, A., and H. Y. McSween, Jr. 1996. Accretionary heating is actually cooling: Why asteroids larger than 4 Vesta did not melt. *Meteor. Planet. Sci.* **31,** A50.

Gooley, R., and C. B. Moore 1976. Native metal in diogenite meteorites. *Am. Mineral.* **61,** 373–378.

Göpel, C., G. Manhès, and C. J. Allègre 1994. U–Pb systematics of phosphates from equilibrated ordinary chondrites. *Earth Planet. Sci. Lett.* **121,** 153–171.

Göpel, C., G. Manhès, and C. J. Allègre 1991. Constraints on the time of accretion and thermal evolution of chondrite parent bodies by precise U–Pb dating of phosphates. *Abstr. 54th Meteor. Soc.*, p. 73.

Greenwood, G. W. 1969. Particle Coarsening. Institute of Metals, London.

Grimm, R. E., and H. Y. McSween, Jr. 1989. Water and the thermal evolution of carbonaceous chondrite parent bodies. *Icarus* **82,** 244–280.

Grimm, R. E., and H. Y. McSween, Jr. 1993. Heliocentric zoning of the asteroid belt by aluminum-26 heating. *Science* **259,** 653–655.

Grossman, L. 1972. Condensation in the primitive solar nebula. *Geochim. Cosmochim. Acta* **38,** 47–64.

Grove, T. L., and K. S. Bartels 1992. The relation between diogenite cumulates and eucrite magmas. *Proc. Lunar Planet. Sci Conf. 22nd* **22,** 437–445.

Haack, H., K. L. Rasmussen, and P. H. Warren 1990. Effects of regolith/megaregolith insulation on the cooling histories of differentiated asteroids. *J. Geophys. Res.* **95,** 5111–5124.

Harlow, G. E., and R. Klimendtis 1980. Clouding of pyroxene and plagioclase in eucrites: Implications for post crystallization processing. *Proc. Lunar. Planet. Sci. Conf. 11th*, 1131–1148.

Hayashi, C., K. Nakazawa, and Y. Nakagawa 1985. Formation of the Solar System. In *Protostars and Planets II* (D. C. Black and M. S. Matthews, Eds.), pp. 1100–1153. Univ. of Arizona Press, Tucson.

Herbert, F. 1989. Primordial electrical induction heating of asteroids. *Icarus* **40,** 484–496.

Herndon, J. M., and M. A. Herndon 1977. Aluminum-26 as a planetoid heat source in the early Solar System. *Meteoritics* **12,** 459–465.

Hertz, H. G. 1968. Mass of Vesta. *Science* **160,** 299–300.

Hewins, R. H. 1981. Orthopyroxene assemblages in diogenites and mesosiderite clasts. *Geochim. Cosmochim. Acta* **45,** 123–126.

Hewins, R. H., and H. E. Newsom 1988. Igneous activity in the early Solar System. In *Meteorites and the Early Solar System* (J. F. Kerridge and M. S. Matthews, Eds.), pp. 73–101. Univ. of Arizona Press, Tucson.

Holzheid, A., and H. Palme 1996. The formation of eucrites as a partial melt from an H-chondrite source: Constraints from new metal silicate partition coefficients. *Meteor. Planet. Sci.* **31,** A63.

Housen, K. R., L. L. Wilkening, C. R. Chapman, and R. J. Greenberg 1990. Regolith development and evolution on asteroids and the Moon. In *Asteroids* (T. Gehrels, Ed.), pp. 65–83. Lunar and Planetary Institute, Houston.

Humayun, M., and R. N. Clayton 1995. Potassium isotope cosmochemistry: Genetic implications of volatile depletions. *Geochim. Cosmochim. Acta* **59,** 2131–2148.

Ikeda, Y., and J. Takeda 1985. A model for the origin of the basaltic achondrites based on the Yamato 7308. *J. Geophys. Res.* **90,** C649–C663.

Jacobsen, S. B., and G. J. Wasserburg 1984. Sm–Nd isotopic evolution of chondrites and achondrites. II. *Geochim. Cosmochim. Acta* **67,** 137–150.

Jones, J. H. 1984. The composition of the mantle of the eucrite parent body and the origin of eucrites. *Geochim. Cosmochim. Acta* **48,** 641–648.

Jones, J. H., D. W. Mittlefehldt, A. J. G. Jurewicz, H. V. Lauer, B. Z. Hanson, C. R. Paslick, and G. A. McKay 1996. The origin of eucrites: An experimental perspective. In *Workshop on Igneous Asteroids: Focus on Vesta and the HED meteorites* (D. W. Mittlefehldt and J. J. Papike, Eds.), pp. 15. Lunar and Planetary Institute, Houston.

Jurewicz, A. J. G., D. W. Mittlefehldt, and J. H. Jones 1995. Experimental partial melting of the St. Severin LL. and Lost City H. chondrites. *Geochim. Cosmochim. Acta* **59,** 391–408.

Keil, K., D. Stoffler, S. G. Love, and E. R. D. Scott 1996. Constraints on the role of impact heating and melting in asteroids. *Meteoritics* **31,** A69–A70.

Labotka, T. C., and J. J. Papike 1980. Howardites: Samples of regolith of the eucrite parent body: Petrology of Frankfort, Pavlovka, Yurtuk, Malvern, and ALHA 77302. *Proc. Lunar. Planet. Sci. Conf. 11th*, 1103–1130.

Langevin, Y., and M. Maurette 1980. A model for small body regolith evolution: The critical parameters. *Proc. Lunar Planet. Sci. Conf. 11th*, 602–604.

Larimer, J. W. 1995. Core formation in asteroid-sized bodies. *Meteoritics* **30,** 552.

LaTourrette, T., and G. J. Wasserburg 1997. Mg diffusion in Anorthite. *Lunar Planet. Sci. Conf. 27th*, 781–782.

Lee, D. C., and A. N. Halliday 1997. Core formation on Mars and differentiated asteroids. *Nature* **388,** 854–857.

Lewis, J. S. 1974. The temperature gradient in the solar nebula. *Science* **186,** 440–443.

Lovering, J. F. 1975. The Moama eurite—A pyroxene–plagioclase adcumulate. *Meteoritics* **10,** 101–114.

Lugmair, G. W., and J. G. Galer 1992. Age and isotopic relationships between angrites Lewis Cliff 86010 and Angra dos Reis. *Geochim. Cosmochim. Acta* **56,** 1673 –1694.

Lugmair, G. W., C. MacIsaac, and A. Shukolykov 1996. Small time differences in different meteorites recorded in the ^{53}Mn-^{53}Cr chronometer. *Lunar Planet. Sci. Conf. 27th*, 813–814.

Lugmair, G. W., and N. B. Scheinin 1975. Sm–Nd systematics of the Stannern meteorite. *Meteoritics* **10,** 447–448.

MacPherson, G. J., A. M. Davis, and E. K. Zinner 1995. The distribution of ^{26}Al in the early Solar System—a reappraisal. *Meteoritics* **30,** 365–386.

Mason, B. 1962. *Meteorites*. Wiley, New York.

McCord, T. B., J. B. Adams, and T. V. Johnson 1970. Asteroid Vesta: Spectral reflectivity and compositional implications. *Science* **168,** 1445–1447.

McCoy, T. J., K. Keil, D. W. Muenow, and L. Wilson 1996. Partial melting and melt migration in the acapulcoite–lodranite parent body. *Geochim. Cosmochim. Acta* **61,** 637–650.

Melosh, H. J. 1990. Early giant impacts and the thermal state of the early earth. In *Origin of the Earth* (H. E. Newsom and J. H. Jones, Eds.), pp. 378. Oxford Univ. Press.

Millis, R. L., and J. L. Elliot 1979. Direct determination of asteroid diameters from occultation observations. In *Asteroids* (T. Gehrels, Ed.), pp. 98–118, Univ. of Arizona Press, Tucson.

Minster, J. F., and C. J. Allégre 1979. ^{87}Rb–^{87}Sr chronology of H chondrites: Constraint and speculations on the early evolution of their parent body. *Earth Planet. Sci. Lett.* **42,** 333–347.

Mittlefehldt, D. W., M. M. Lindstrom, D. D. Bogard, D. H. Garrison, and S. W. Field 1996. Acapulco- and Lodran-like achondrites: Petrology, geochemistry, chronology and origin. *Geochim. Cosmochim. Acta* **60,** 867–882.

Miyamoto, M., M. B. Duke, and D. S. McKay 1985. Chemical zoning and homogenization of Pasamonte-type pyroxene and their bearing on thermal metamorphism of a howardite parent body. *J. Geophys. Res.* **90,** C629–C635.

Miyamoto, M., N. Fujii, and H. Takeda 1981. Ordinary chondrite parent body: An internal heating model. *Proc. Lunar Planet. Sci. Conf. 12th*, 1145–1152.

Navrotsky, A. 1994. *Physics and Chemistry of Earth Materials.* Cambridge Univ. Press, Cambridge.

Newsom, H. E. 1985. Molybdenum in eucrites: Evidence for a metal core in the eucrite parent body. *Proc. Lunar. Planet. Conf.* **15,** C613–C617.

Newsom, H. E. 1996. Core formation in the Howardite-Eucrite-Diogenite Parent Body. In *Workshop on Igneous Asteroids: Focus on Vesta and HED Meteorites* (D. W. Mittlefehldt and J. J. Papike, Eds.), p. 44. Lunar Planetary Institute.

Newsom, H. E., and M. J. Drake 1982. The metal content of the eucrite parent body: Constraints from the partitioning of Tungsten. *Geochim. Cosmochim. Acta* **43,** 989–1007.

Nyquist, L. E., H. Takeda, B. M. Bansal, C. Y. Shih, H. Weismann, and J. L. Wooden 1986. Rb–Sr and Sm–Nd isochron ages of a subophitic basaltic clast and a matrix sample from the Y75011 eucrite. *J. Geophys. Res.* **91,** 8137–8150.

Palme, H., and W. Rammensee 1981. The cosmic abundance of molybdenum. *Earth Planet. Sci. Lett.* **55,** 356–362.

Papanastassiou, D. A., and G. J. Wasserburg 1969. Initial strontium isotopic abundances and the resolution of small time differences in the formation of planetary bodies. *Earth Planet. Sci. Lett.* **5,** 361–376.

Podosek, F. A., and P. Cassen 1994. Theoretical, observational, and isotopic estimates of the lifetime of the solar nebula. *Meteoritics* **29,** 6–25.

Reed, K. L., M. J. Gaffey, and L. A. Lebofsky 1996. Shape and albedo variations of asteroid 4 Vesta. In *Workshop on Evolution of Igneous Asteroids: Focus on Vesta and the HED Meteorites* (D. W. Mittlefehldt and J. J. Papike, Eds.), pp. 22–23, Lunar and Planetary Institute, Houston.

Righter, K., and M. J. Drake 1997. Formation of eucrites and diogenites by equilibrium crystallization in a chondritic magma ocean. *Meteor. Planet. Sci.* **32,** A109.

Robie, R. A., B. S. Hemmingway, and J. R. Fisher 1978. Thermodynamic properties of minerals and related substances at 298.15 K and 1 bar pressure and at higher temperature. *Geol. Surv. Bull.* 1452.

Ruzicka, A., G. A. Snyder, and L. A. Taylor 1996. Asteroid 4 Vesta as the HED parent body: Implications for a metallic core and magma ocean crystallization. In *Workshop on Igneous Asteroids: Focus on Vesta and the HED Meteorites* (D. W. Mittlefehldt and J. J. Papike, Eds.), pp. 23–24. Lunar and Planetary Institute, Houston.

Schramm, D. N., F. Tera, and G. J. Wasserburg 1970. The isotopic abundance of ^{26}Mg and limits on ^{26}Al in the early Solar System. *Earth Planet. Sci. Lett.* **10,** 44–59.

Schubart, J., and D. L. Matson 1979. Masses and densities of asteroids. In *Asteroids* (T. Gehrels, Ed.), pp. 84–97. Univ. of Arizona Press, Tucson.

Shukolyukov, A., and G. W. Lugmair 1993. Iron-60 in eucrites. *Earth Planet. Sci. Lett.* **119,** 154–166.

Shukolyukov, A., and G. W. Lugmair 1997. ^{60}Fe–^{60}Ni systematics in the eucrite Caldera. *Meteoritics* **31,** A129.

Standish, E. M., and R. W. Hellings 1989. A determination of the masses of Ceres, Pellas and Vesta from their perturbations upon the orbit of Mars. *Icarus* **80,** 326–333.

Stevenson, D. J. 1981. Models of the Earth's core. *Science* **214,** 611–619.

Stolper, E. 1977. Experimental petrology of eucritic meteorites. *Geochim. Cosmochim. Acta* **41,** 587–611.

Takeda, H., H. Mori, J. S. Prinz, G. E. Harlow, and T. Ishii 1983. Mineralogical comparison of Antarctic and non-Antarctic HED howardites–eucrites–diogenites. *Proc. Symp. Antarct. Meteorites* **8,** 114–116.

Tatsumoto, M., R. J. Knight, and C. J. Allegre 1973. Time differences in the formation of meteorites as determined from the ratio of lead-207 to lead-206. *Science* **180,** 1279–1283.

Taylor, G. J. 1992. Core formation in asteroids. *J. Geophys. Res.* **97,** 14,717–14,726.

Taylor, S. R., and M. D. Norman 1990. Accretion of differentiated planetesimals to the earth. In *The Origin of the Earth* (H. E. Newsom and J. J. Jones, Eds.), Oxford Univ. Press, New York.

Tedesco, E. F. 1989. Asteroid magnitudes, UBV colors and IRAS albedos and diameters. In *Asteroids II*, pp. 997–1001. Univ. of Arizona Press, Tucson.

Tera, F., R. W. Carlson, and N. Z. Boctor 1989. Contrasting Pb–Pb ages of the Cumulate and Noncumulate Eucrites. *Lunar Planet. Sci. Conf. 20th*, 1111–1112.

Tera, F., R. W. Carlson, and N. Z. Boctor 1997. Radiometric ages of basaltic achondrites and their relation to the early history of the Solar System. *Geochim. Cosmochim. Acta* **61,** 1713–1732.

Thomas, P. C., R. P. Binzel, M. J. Gaffey, A. D. Storrs, E. N. Wells, and B. H. Zellner 1997a. Impact excavation on asteroid 4 Vesta: Hubble Space Telescope results. *Science* **277,** 1492–1495.

Thomas, P. C., R. P. Binzel, M. J. Gaffey, B. H. Zellner, A. D. Storrs, and E. Wells 1997b. Vesta: Spin pole, size and shape for the HST images. *Icarus* **128,** 88–94.

Treiman, A. H., and M. J. Drake 1985. Basaltic volcanism on the eucrite parent body: Petrology and chemistry of the polymict eucrite ALH80102. *J. Geophys. Res.* **90,** C619–C628.

Turcotte, D. L., and G. S. Schubert 1982. *Geodynamics.* Wiley, New York.

Weidenschilling, S. J. 1988. Formation processes and time scales for meteorite parent bodies. In *Meteorites and the Early Solar System* (J. F. Kerridge and M. S. Matthews, Eds.), pp. 348–371. Univ. of Arizona Press, Tucson.

Wetherill, G. W. 1987. Dynamical relations between asteroids, meteorites and Apollo–Amor objects. *Phil. Trans. R. Soc. London A* **323,** 323–337.

White, F. M. 1995. *Fluid Mechanics.* McGraw-Hill, New York.

Williams, D. R., and G. W. Wetherill 1993. Equilibrium models of mass distribution and collisional lifetime of asteroids. *Lunar Planet. Sci. Conf. 24th*, 1523–1524.

Wilson, L. L., and K. Keil 1996. The nature of volcanic eruptions on 4 Vesta. In *Workshop on Igneous Asteroids: Focus on Vesta and HED Meteorites* (D. W. Mittlefehldt and J. J. Papike, Eds.), p. 44. Lunar Planetary Institute.

Wisdom, J. 1985. A perturbative treatment of motion near 3/1 commensurability. *Icarus* **63,** 272–289.

Wood, J. A. 1979. Review of the metallographic cooling rates of meteorites and a new model for the planetesimals in which they formed. In *Asteroids* (T. Gehrels, Ed.), pp. 849–891. Univ. of Arizona Press, Tucson.

Wood, J. A., and G. E. Morfill 1988. A review of solar nebula models. In *Meteorites and the Early Solar System* (J. F. Kerridge and M. S. Matthews, Eds.), pp. 328–347. Univ. Arizona Press, Tucson.

Wood, J. A., and P. Pellas 1991. What heated the parent meteorite planets? In *The Sun in Time* (C. P. Sonnett and M. S. Giampapa, Eds.), pp. 740–760. Univ. Arizona Press, Tucson.

Yamaguchi, A., G. Taylor, and K. Keil 1996. Global crustal metamorphism of the eucrite parent body. *Nature* **124,** 97–112.

Yomogida, K., and T. Matsui 1983. Physical properties of ordinary chondrites. *J. Geophys. Res.* **88,** 9513–9533.

Zolensky, M. E., M. K. Weisberg, P. C. Buchanan, and D. W. Mittlefehldt 1996. Carbonaceous chondrite clasts in HED achondrites. In *Workshop on Evolution of Igneous Asteroids: Focus on Vesta and the HED Meteorites* (D. W. Mittlefehldt and J. J. Papike, Eds.), pp. 43–44. Lunar and Planetary Institute, Houston.